46.2 ± 19.2 years and the mean disease duration at examination was 7.5 ± 8.1 years. Clinical classification was graded based on the worst condition of each patient according to the Task Force of the Medical Advisory Board of the Myasthenia Gravis Foundation of America; There were 104 patients in class 1 (ocular), 114 in class 2 (mild generalized), 75 in class 3 (moderate generalized), 13 in class 4 (severe generalized), and 30 in class 5 (crisis) (Jaretzki et al., 2000). Extended thymectomy was performed in 149 patients, and histopathologic examination revealed 71 patients with thymoma. 226 patients were positive for anti-AChR antibodies. An assay for anti-MuSK antibodies was further performed in AChR-seronegative patients and 3 patients were positive. Serum anti-titin antibodies were measured by enzyme-linked immunosorbent assay (ELISA). HLA class II DRB1 alleles were determined based on polymerase chain reaction and a restriction fragment method using genomic DNA extracted from peripheral blood leukocytes. Clinical information including the presence of additional autoimmune diseases was retrospectively obtained for all MG patients by reviewing their clinical charts. As diseases controls and normal controls, we used serum samples from 28 patients with Duchenne muscular dystrophy (DMD), 20 patients with thymoma without MG and 28 healthy volunteers. In addition, muscle tissues were obtained from 5 patients who were followed at Kanazawa University. All clinical samples and information were collected after the patients and controls gave their written informed consent as approved by the institutional review boards of each hospital.

2.2. Immunoprecipitation assay

Serum autoantibodies were screened by immunoprecipitation assay using ^{35}S-labeled RD cellular extracts (Suzuki et al., 2005). RD cells (2×10^5 per sample) were cultured in methionine-free DMEM (Sigma, St. Louis, MO) containing 3% heat-inactivated fetal bovine serum in the presence of 20 μCi/ml ^{35}S-methionine for 14 h. The ^{35}S-labeled cells were resuspended in an ice-cold buffer containing 500 mM NaCl, 0.1% Nonidet P-40, 10 mM Tris–HCl, and a cocktail of protease inhibitors (COMPLETE; Roche, Mannheim, Germany), and sonicated intermittently on ice for a total of 90 s. The supernatant, containing ^{35}S-labeled soluble proteins originating from the nuclei, cytoplasm, and cellular membrane, was recovered by centrifugation (13,000 *g* for 15 min) and used as the antigen source. Two milligrams of protein A-Sepharose CL-4B (Pharmacia Biotech, Stockholm, Sweden) was incubated with 10 μl of a human serum sample. The immunoglobulins that were bound to protein A-Sepharose beads were then incubated with the ^{35}S-labeled cellular extracts for 2 h. The immunoprecipitated material was resolved by electrophoresis on SDS—7.5% polyacrylamide gels, which were subsequently treated with 0.5 M sodium salicylate to enhance the radioactivity, and evaluated by autoradiography using a BAS-5000 system (Fuji Film, Tokyo, Japan).

2.3. Affinity-purification and identification of the autoantigen

The antigens recognized by patients' sera were isolated from the RD extracts by affinity-purification (Suzuki et al., 2005). A mixture of MG sera containing the antibody of interest (0.5 ml) was incubated with protein A-Sepharose CL-4B (0.5 g), and the antibody-protein A complex was cross-linked by treatment with dimethylpimelimidate (Pierce, Rockford, IL). The cellular extracts derived from RD cells (2.5×10^8) were incubated with the antibody–protein A bead complex, and proteins that bound to the antibodies were eluted using a buffer containing 3 M $MgCl_2$ and 1 mM DTT. The eluted materials were dialyzed against PBS, concentrated using an Ultrafree-4 Centrifugal Filter (Millipore, Billerica, MA), and fractionated on SDS—7.5% polyacrylamide gels, followed by Coomassie blue staining. Excised plugs from Coomassie-stained gels were analyzed by matrix-assisted laser desorption/ionization-time of flight (MALDI-TOF) mass spectroscopy at APRO Science (Tokushima, Japan) (Ozaki et al., 2004). The obtained peptide mass fingerprint spectra were then analyzed be searching the National Center for Biotechnology Information.

2.4. Immunoblots

Antigenicity of the affinity-purified preparation was examined by immunoblots (Suzuki et al., 2005). Proteins were fractionated on SDS-10% polyacrylamide gels and transferred to nitrocellulose membranes. They were blocked with 5% non-fat milk and incubated with serum samples diluted 1:250, rabbit anti-GRP94 polyclonal antibodies diluted 1:200 (Stressgen, Victoria, Canada), or rabbit polyclonal antibodies to an irrelevant antigen as a control.

2.5. Indirect immunofluorescence

RD cells were grown on fibronectin-coated chamber slides (Becton Dickinson Labware, Bedford, MA). After a 24-hour culture, the cells were fixed with 4% paraformaldehyde for 5 min. The cells were then incubated with serum samples diluted 1:20, rabbit anti-GRP94 polyclonal antibody diluted 1:100, or control rabbit antibodies.

2.6. ELISA

96-well polyvinyl plates (Smilon multiwell plate H type; Sumitomo Bakelite, Tokyo, Japan) were coated with recombinant GRP94 protein (Prospec, Rehovot, Israel) at 0.5 μg/ml diluted in Antigen Coating Buffer (ImmunoChemistry Technologies, Bloomington, MN) (Kuwana et al., 2002). The remaining blocking sites were blocked with General Low Level Blocker with BSA (ImmunoChemistry Technologies). Sera were dilated 1:100 in phosphate-buffered saline containing 0.1% bovine serum albumin. The wells were incubated with serum samples and subsequently with peroxidase-conjugated anti-human IgG (Cappel, Aurora, OH) diluted 1:5000. The antibody binding was visualized by incubation with tetramethylbenzidine (1 mg/ml) in phosphate–citrate buffer. The reaction was stopped by 1 M sulfuric acid. The optical density at 450 nm (OD450) was read with an automatic plate reader (Biorad, Hercules, CA). Samples were tested in duplicate. The antibody index was calculated from the OD450 of the samples divided by the OD450 of the standard serum containing for the anti-90 kDa antibody.

2.7. Immunohistochemistry

At the extended thymectomy, tissue samples were taken from the musculus pectoralis major, and immediately frozen in liquid nitrogen cooled isopentane (Iwasa et al., 2010). Six micrometer sections of frozen tissue from MG patients and controls were prepared and fixed briefly in cold acetone. The sections were incubated with rabbit anti-GRP94 polyclonal antibodies diluted 1:400.

2.8. Statistical analyses

Statistical analysis was performed using a statistical software program (StatView 5.0; SAS Institute Inc. Cary, NC). Comparisons for relative frequencies between 2 groups were tested for statistical significance using the chi-square test or Fisher's 2-tailed exact test for 2×2 tables. Continuous variables were compared using Student's *t*-test. Disease severity was compared by the Mann–Whitney test. Values of $p<0.05$ were considered to indicate statistical significance.

3. Results

3.1. Detection of autoantigens by immunoprecipitation assay

We subjected the sera of 336 patients with MG, and 48 disease controls (28 patients with DMD and 20 with thymoma without MG) and

28 healthy controls to the immunoprecipitation assay using ^{35}S-labeled RD extracts as antigen sources. Representative results obtained from MG and control sera are shown in Fig. 1. Several immunoprecipitated proteins were detected in MG sera, but fewer were detected in control sera. Among these autoantigens, those with relatively intense immunoprecipitated protein bands having a molecular weight of 70-kDa had already been identified as Kv1.4 (Suzuki et al., 2005). The 90-kDa autoantigens were recognized in 24 (7.1%) of 336 MG sera, but in none of the diseases control or healthy control sera ($p = 0.01$). Since the 90-kDa protein was specifically and frequently detected in the MG sera, we focused on this autoantigen in the following analysis.

3.2. Identification of the 90-kDa autoantigen as GRP94

The 90-kDa protein was successfully isolated from the RD extracts by affinity-purification using MG sera that contained an antibody to this protein. The portion of the gel corresponding to the 90-kDa protein was cut out and subjected to MALDI-TOF mass spectroscopy. The mass spectroscopy detected 9 different peptides that together covered 19% of the human GRP94 protein (accession number NM_003299) (Table 1). This finding identified the protein to be human GRP94 with a degree of probability (MOWSE Score: 4.68e + 0.05). The predicted molecular weight of human GRP94 was 92.4 kDa, which was consistent with that observed in the immunoprecipitation assay.

A series of experiments was then carried out to test whether the 90-kDa protein targeted by the MG sera was truly GRP94. First, the affinity-purified 90-kDa protein was subjected to immunoblotting as an antigen source (Fig. 2A). The 90-kDa protein was successfully recognized by the rabbit anti-GRP94 polyclonal antibody, but not by a control rabbit antibody (lanes 1, 2). We further examined the reactivity to the 90-kDa protein in 4 MG serum samples containing

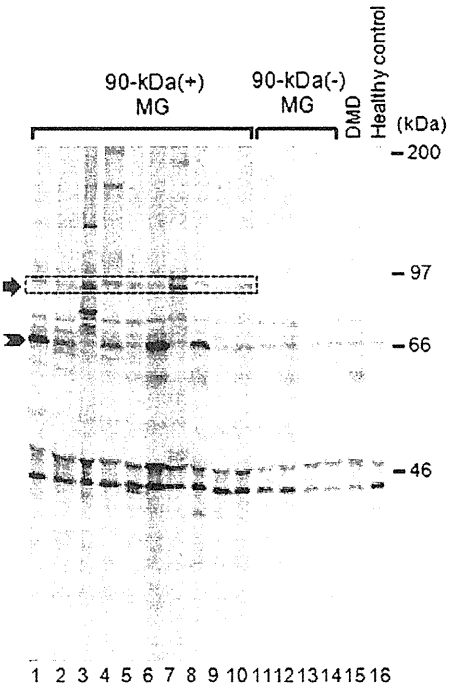

Fig. 1. Immunoprecipitation assay. Autoradiograms of immunoprecipitated ^{35}S-labeled RD extracts from the serum samples of myasthenia gravis (MG) patients (lanes 1–14), a Duchenne muscular dystrophy (DMD) patient (lane 15) and a healthy control (lane 16) are shown. Immunoprecipitated materials were analyzed on SDS–7.5% polyacrylamide gels. The positions of the molecular weight standards appear to the right of the panel. The arrow indicates the 90-kDa precipitate detected in the serum sample of MG patients (lanes 1–10). The arrowhead indicates the Kv1.4 at the molecular sizes of 70-kDa.

Table 1
Mass spectroscopy of the 90-kD band: the matched peptide of GRP94.

Measured Mass (M)	Computed Mass	Error (%)	Residues	Sequence of matched peptide
1081.5462	1081.5431	+0.0002	76–84	FAFQAEVNR
1306.6463	1306.6506	−0.0004	614–623	EFEPLLNWMK
1762.8522	1762.8441	+0.0004	480–493	YNDTFWKEFGTNIK
1786.8870	1786.9122	−0.0015	141–156	EKNLLHVTDTGVGMTR
2260.0565	2260.0634	−0.0003	512–530	FQSSHHPTDISSLDQYVER
2370.1057	2370.0858	+0.0008	640–660	LTESPCALVASQYGWSGNMER
2542.2877	2542.2917	−0.0002	329–348	TVWDWELMNDIKPIWQRPSK
2711.2321	2711.2086	+0.0008	215–237	HNNDTQHIWESDSNEFSVIADPR
2782.2861	2728.3090	−0.0008	44–67	TDDEVVQREEEAIQLDGLNASQIR

the anti-90-kDa antibody, 4 serum samples lacking the anti-90-kDa antibody, and 2 DMD and 2 healthy control serum samples. Among these sera, the samples positive for anti-90-kDa antibody reacted with the affinity-purified 90-kDa protein by immunoblots, but not the others (lanes 3–7).

Second, indirect immunofluorescence (Fig. 2B) showed that RD cells were incubated with the rabbit anti-GRP94 antibody (red) and MG sera that contained or lacked the anti-90-kDa antibody (green). A representative serum sample that contained the anti-90-kDa antibody produced membranous and cytoplasmic staining on cells that overlapped with staining by the anti-GRP94 antibody (upper panel). Similar findings were observed using 3 additional MG serum samples containing the anti-90-kDa antibody. In contrast, serum samples from 4 MG patients that lacked the anti-90-kDa antibody and 2 healthy controls did not show any staining on the RD cells (middle and lower panels). Specificity of the staining was confirmed by the lack of staining on RD cells with control rabbit antibody.

Finally, autoimmunity to the 90-kDa protein was further evaluated by ELISA using recombinant GRP94 protein as the antigen source. A total of 142 serum samples were examined. The anti-GRP94 antibody index was significantly higher in the 24 serum samples containing the anti-90-kDa antibody than the other groups, including the 42 MG patients lacking anti-90-kDa antibody, the 20 thymoma patients without MG, the 28 DMD patients and the 28 healthy controls (Fig. 2C). When the cut-off value was set as the mean + 5 SD of healthy control sera, positivity for the anti-GRP94 antibody was observed in 92% of MG patients containing the anti-90-kDa antibody, but not in either MG patients lacking the anti-90-kDa antibody, thymoma patients without MG or in DMD patients ($p < 0.001$).

Taken together, these findings indicate that the 90-kDa protein detected by the immunoprecipitation assay was really GRP94.

3.3. Clinical features defined by the anti-GRP94 antibody in MG patients

Demographic and clinical findings were compared between 24 MG patients with the anti-GRP94 antibody and 312 MG patients without the antibody (Table 2). There was no difference in gender or age at MG onset. There were also no significant differences in the disease subsets by MGFA clinical classification. Thymoma was more frequent in the anti-GRP94-positive than in the anti-GRP94-negative patients ($p = 0.04$). In regard to the coexistence of MG-related antibodies, there were no differences in the frequencies of anti-AChR or anti-MuSK antibodies between the two groups. In contrast, anti-titin and anti-Kv1.4 antibodies were detected in 25% and 13% of the 336 MG patients, respectively. The frequencies of anti-titin and anti-Kv1.4 antibodies were higher in the anti-GRP94-positive than in the anti-GRP94-negative patients ($p = 0.004$ and 0.003, respectively).

Of the 336 MG patients, 50 (14.8%) developed additional autoimmune diseases. It was noted that the frequency of associated autoimmune diseases was much higher in the anti-GRP94-positive than in the anti-GRP94-negative patients (71% versus 11%, $p < 0.001$). Table 3 shows the clinical and immunological features in these 17 MG

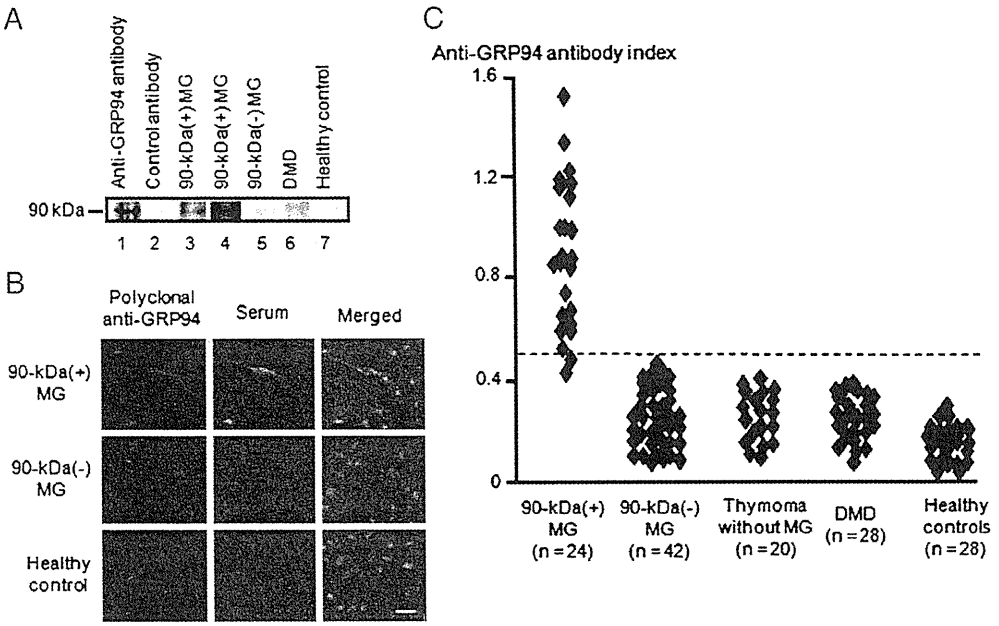

Fig. 2. Identification of the 90-kDa autoantigen as GRP94. (A) Immunoblots using an affinity-purified 90-kDa protein antigen. The affinity-purified 90-kDa was analyzed on a SDS-10% polyacrylamide gel, and probed with rabbit polyclonal anti-GRP94 antibody (lane 1), control rabbit antibody (lane 2), myasthenia gravis (MG) serum with anti-90-kDa antibody (lane 3, 4), MG serum without anti-90-kDa antibody (lane 5), Duchenne muscular dystrophy (DMD) serum (lane 6) or healthy control serum (lane 7). (B) Indirect immunofluorescence of muscle cells subjected to double-staining with rabbit polyclonal anti-GRP94 antibody (red) and sera from MG patients with or without anti-90-kDa antibodies or healthy controls (green). The cells were examined with a confocal laser fluorescent microscope. The bar indicates 10 μm. (C) Antibodies reactive with recombinant GRP94 protein by enzyme-linked immunosorbent assay in sera from anti-90-kDa-positive MG patients, anti-90-kDa-negative MG patients, thymoma patients without MG, DMD patients, and healthy controls. The cut-off level for positivity is indicated by the broken line.

patients with anti-GRP94 antibody accompanied by other autoimmune diseases. They consisted of 3 men and 14 women of various ages and with various MG symptoms. Seven patients had thymoma-associated MG. It was likely that DRB1 alleles and additional autoimmune diseases were heterogeneous. In 8 of 17 patients, MG preceded the other autoimmune diseases or developed at the same time. In contrast, 9 patients who had already suffered from other autoimmune diseases had an additional diagnosis of MG. It was noted that the other autoimmune diseases were generally well controlled or in remission.

Table 2
Demographic and clinical findings in MG patients with or without serum anti-GRP94 antibody.

	Anti-GRP94 positive (n=24)	Anti-GRP94 negative (n=312)	p
Women (%)	79	64	NS
Age at disease onset (years; mean ± SD)	46.2 ± 19.5	46.0 ± 15.4	NS
MG Foundation of America classification (%)			NS
Ocular (class 1)	21	32	
Mild generalized (class 2)	29	34	
Moderate generalized (class 3)	29	22	
Severe generalized (class 4)	4	4	
Crisis (class 5)	17	8	
Bulbar involvement (%)	50	37	NS
Thymoma (%)	38	20	0.04
Coexistent MG-related antibodies (%)			
Anti-acetylcholine receptor antibody	88	66	NS
Anti-MuSK antibody	0 (0/3)	3 (3/107)	NS
Anti-titin antibody	50	23	0.004
Anti-Kv1.4 antibody	33	12	0.003
Additional autoimmune diseases (%)	71	11	<0.001

Abbreviations: MG = myasthenia gravis; MuSK = muscle-specific receptor tyrosine kinase; NS = not significant.

3.4. Expression of GRP94 in the muscles of MG patients

The expression of GRP94 was examined in the muscle tissues from MG and disease controls using immunohistochemistry. The GRP94 immunoreactivity was evaluated based on positive in the results from patients with inclusion body myositis (IBM) and negative in those from patients with peripheral neuropathy (Fig. 3A, B). The results showed that 4 of the 5 patients with MG exhibited clear GRP94 expression. GRP94 immunoreactivity was clearly stained mainly on the surface of the muscle fibers (Fig. 3C), compared to negatively stained (Fig. 3D).

4. Discussion

We identified an autoantibody to GRP94, one of the ER chaperones, in 7.1% of the MG serum samples examined in this study. The identification of the 90-kDa autoantigen targeted by MG sera as GRP94 was based on MALDI-TOF mass spectroscopy. This finding was strengthened by the following results: (i) polyclonal anti-GRP94 antibody reacted with the affinity-purified 90-kDa antigen; (ii) MG sera containing the anti-90-kDa antibody and anti-GRP94 polyclonal antibody exclusively stained RD cells; and (iii) ELISA using a recombinant GRP94 protein showed that MG serum samples containing the anti-90-kDa antibody exhibited markedly higher levels of anti-GRP94 antibody than the serum samples lacking this antibody. Of the 336 MG patients, 50 (14.8%) developed additional autoimmune diseases. Importantly, the frequency of associated autoimmune diseases was much higher in the anti-GRP94-positive than the anti-GRP94-negative patients (71% versus 11%, $p<0.001$). Clinical feature defined by the anti-GRP94 antibody is a new subset of MG. In addition, we demonstrated that GRP94 was expressed in the muscle tissues of patients with MG.

Recently, it was reported that dysregulation of the UPR may participate in the development of autoimmunity (Todd et al., 2008).

Table 3
Clinical and immunological features in 17 anti-GRP94-positive MG patients with additional autoimmune diseases.

No/sex/age at MG onset	MGFA class	Thymus (thymoma type)	AChR Ab (nM)	DRB1 alleles	Autoimmune diseases (age at disease onset)
1/M/20	3b	Thymoma (B2)	290	0403/0901	Alopecia and vitiligo (22)
2/F/23	2a	Hyperplasia	45	0405/0901	Hashimoto disease (21)
3/F/24	3b	Atrophy	355	0901/1302	Antiphospholipid antibody syndrome (21)
4/F/28	2a	Hyperplasia	556	0405/0803	Basedow disease (15)
5/F/35	3b	Atrophy	81	0901/1302	Systemic lupus erythematosus (35)
6/F/36	2a	Thymoma (B1)	160	0803/1201	Hashimoto disease (29)
7/F/48	2a	No	88	1501/0803	Rheumatoid arthritis (46)
8/F/48	5	No	94	1301/1501	Sarcoidosis (48)
9/F/51	2b	No	44	1406/1501	Hashimoto disease (54)
10/F/52	1	Thymoma (B3)	17	0405/0901	Mixed connective tissue disease (52)
11/F/54	3b	Thymoma (B3)	180	0802/1201	Aplastic anemia (59)
12/F/56	1	No	0	0803/0901	Hashimoto disease (54)
13/M/58	5	Thymoma (B2)	68	ND	Hashimoto disease (31)
14/M/59	3b	Thymoma (B1)	34	ND	Hashimoto disease (59)
15/F/67	1	No	0	0101/0803	Sarcoidosis (62)
16/F/68	3a	Thymoma (B1)	132	0101/1502	Pure red cell aplesia (69)
17/F/68	4b	No	150	0803/1403	Myositis (66)

Abbreviations: AChR Ab = acetylcholine receptor antibody; MG = myasthenia gravis; MGFA = myasthenia gravis foundation of America; ND = not detected.

Some models support the idea that inadequate UPR contributes to autoimmune diseases through several mechanisms. First, recognition of misfolded proteins may be immunogenic. Abnormally folded HLA-B27 molecules can be expressed on the cell surface and have been postulated to induce an autoimmune response in ankylosing spondylitis (Turner et al., 2007). Second, UPR-related proteins may act as autoantigens. In patients with rheumatoid arthritis, BIP is overexpressed in cells in the synovium that preferentially stimulated autoreactive T cells. Autoantibodies against BIP are also detected in their sera (Corrigall et al., 2001). Finally, UPR-related proteins may act as an immune adjuvant and elicit immune response in a mouse model of Sjögren's syndrome (Purcell et al., 2003).

The relation between GRP94 and autoimmune diseases has been studied by several groups. GRP94 transgenic mice develop lupus-like autoimmune diseases and systemic inflammation associated with cell surface expression of GRP94 by activating autoreactive T cells (Liu et al., 2003). It is suggested that chronic stimulations by extracellular GRP94 may contribute to a novel mechanism of autoimmune diseases (Liu et al., 2003). In fact, autoantibodies to GRP94 are also detected in patients with systemic lupus erythematosus (Boehm et al., 1994). In addition, the plasma concentration of GRP94 is markedly increased in autoimmune diabetic patients (Pagetta et al., 2003). In the present study, we did not examine the autoimmunity to GRP94 in patients with other autoimmune diseases. However, based on previous

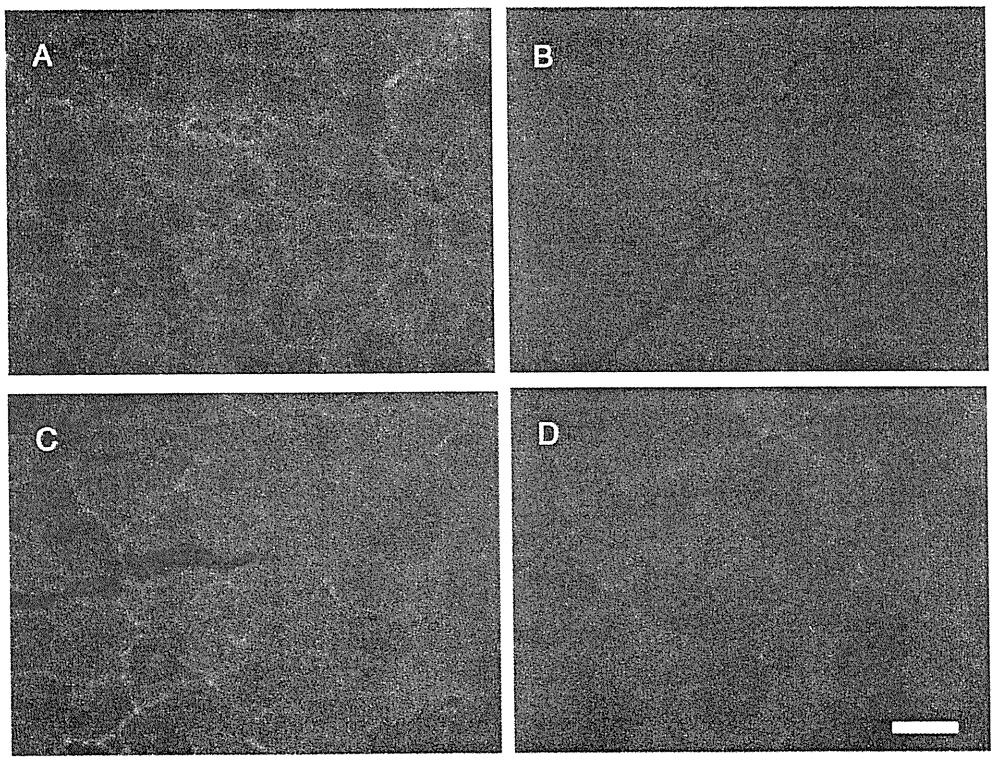

Fig. 3. Grp94 immunoreactivity in MG muscles. Sections were obtained from patients with inclusion body myositis (A), peripheral neuropathy (B) and myasthenia gravis (MG) (C, D). GRP94 was expressed on the surface of muscle cells in the MG patient (C) as well as the positive control (A), but no immunoreactivity in the other patient (D). The bar indicates 100 μm.

reports, we believe that the autoimmunity to endoplasmic reticulum chaperone GRP94 may possibly hold the significance to primarily a marker of autoimmunity in general.

Various autoimmune diseases are associated with thymoma (Evoli et al., 2007). It is well known that thymomas of the AB and B types are mainly associated with MG and other autoimmune diseases. In fact, all thymoma in 7 MG patients with anti-GRP94 antibody were type B. These findings may suggest that type B thymoma can export T cells to the periphery. In contrast, there was no autoimmunity to GRP94 in thymoma without autoimmune diseases. Moreover, several anti-striational autoantibodies are frequently detected in thymoma-associated with MG (Meriggioli and Sanders, 2009). We think that the association between anti-GRP94 antibody and anti-striational antibodies including titin and Kv1.4 may primarily be due to the presence of thymoma.

Skeletal muscle can actively participate in local immune reactions with a variety of immunologically important molecules (Wiendl et al., 2005). The UPR is also closely related to the immune reactions of inflammatory myopathies. ER chaperones including BIP and GRP94 are found to be accumulated in IBM muscle fibers (Vattemi et al., 2004). Moreover, the UPR is significantly activated in the muscle tissues of human myositis and its mouse model (Nagaraju et al., 2005). Although the main target of the autoimmune reaction in MG is the neuromuscular junction, the skeletal muscle itself is also associated with the pathogenesis of MG (Iwasa et al., 2010). The immune response may be caused by certain types of MG-related muscle autoantigens, such as titin, ryanodine receptor and Kv1.4 (Suzuki et al., 2009). As a result of ER stress, GRP94 is expressed in MG muscles and may act as an autoantigen targeted by MG sera (Corrigall et al., 2001; Liu et al., 2003).

In conclusion, autoimmunity to ER chaperon GRP94 is associated with a subset of MG patients who have additional autoimmune diseases.

Acknowledgments

This work was supported by a grant from the Japanese Ministry of Education, Science, Sports and Culture (no. 23591255) and a Neuroimmunological Disease Research Committee grant from the Japanese Ministry of Health, Labour, and Welfare.

References

Boehm, J., Orth, T., Van Nguyen, P., Soling, H.D., 1994. Systemic lupus erythematosus is associated with increased auto-antibody titers against calreticulin and grp94, but calreticulin is not the Ro/SS-A antigen. Eur. J. Clin. Invest. 24, 248–257.

Corrigall, V.M., Bodman-Smith, M.D., Fife, M.S., Canas, B., Myers, L.K., Wooley, P., Soh, C., Staines, N.A., Pappin, D.J., Berlo, S.E., van Eden, W., van Der Zee, R., Lanchbury, J.S., Panayi, G.S., 2001. The human endoplasmic reticulum molecular chaperone BiP is an autoantigen for rheumatoid arthritis and prevents the induction of experimental arthritis. J. Immunol. 166, 1492–1498.

Evoli, A., Minicuci, G.M., Vitaliani, R., Battaglia, A., Della Marca, G., Lauriola, L., Fattorossi, A., 2007. Paraneoplastic diseases associated with thymoma. J. Neurol. 254, 756–762.

Iwasa, K., Kato-Motozaki, Y., Furukawa, Y., Maruta, T., Ishida, C., Yoshikawa, H., Yamada, M., 2010. Up-regulation of MHC class I and class II in the skeletal muscles of myasthenia gravis. J. Neuroimmunol. 225, 171–174.

Jaretzki III, A., Barohn, R.J., Ernstoff, R.M., Kaminski, H.J., Keesey, J.C., Penn, A.S., Sanders, D.B., 2000. Myasthenia gravis: recommendations for clinical research standards. Task Force of the Medical Scientific Advisory Board of the Myasthenia Gravis Foundation of America. Neurology 55, 16–23.

Kuks, J.N.M., Oosterhuis, H.J.G.H., 2003. Clinical Presentation and Epidemiology of Myasthenia Gravis. In: Kaminski, H.J. (Ed.), Myasthenia gravis and related disorders. Humana Press, New Jersey, pp. 93–113.

Kuwana, M., Kimura, K., Kawakami, Y., 2002. Identification of an immunodominant epitope on RNA polymerase III recognized by systemic sclerosis sera: application to enzyme-linked immunosorbent assay. Arthritis Rheum. 46, 2742–2747.

Liu, B., Dai, J., Zheng, H., Stoilova, D., Sun, S., Li, Z., 2003. Cell surface expression of an endoplasmic reticulum resident heat shock protein gp96 triggers MyD88-dependent systemic autoimmune diseases. Proc. Natl. Acad. Sci. U. S. A. 100, 15824–15829.

Meriggioli, M.N., Sanders, D.B., 2009. Autoimmune myasthenia gravis: emerging clinical and biological heterogeneity. Lancet Neurol. 8, 475–490.

Nagaraju, K., Casciola-Rosen, L., Lundberg, I., Rawat, R., Cutting, S., Thapliyal, R., Chang, J., Dwivedi, S., Mitsak, M., Chen, Y.W., Plotz, P., Rosen, A., Hoffman, E., Raben, N., 2005. Activation of the endoplasmic reticulum stress response in autoimmune myositis: potential role in muscle fiber damage and dysfunction. Arthritis Rheum. 52, 1824–1835.

Ozaki, K., Inoue, K., Sato, H., Iida, A., Ohnishi, Y., Sekine, A., Sato, H., Odashiro, K., Nobuyoshi, M., Hori, M., Nakamura, Y., Tanaka, T., 2004. Functional variation in LGALS2 confers risk of myocardial infarction and regulates lymphotoxin-alpha secretion in vitro. Nature 429, 72–75.

Pagetta, A., Folda, A., Brunati, A.M., Finotti, P., 2003. Identification and purification from the plasma of Type 1 diabetic subjects of a proteolytically active Grp94Evidence that Grp94 is entirely responsible for plasma proteolytic activity. Diabetologia 46, 996–1006.

Purcell, A.W., Todd, A., Kinoshita, G., Lynch, T.A., Keech, C.L., Gething, M.J., Gordon, T.P., 2003. Association of stress proteins with autoantigens: a possible mechanism for triggering autoimmunity? Clin. Exp. Immunol. 132, 193–200.

Suzuki, S., Satoh, T., Yasuoka, H., Hamaguchi, Y., Tanaka, K., Kawakami, Y., Suzuki, N., Kuwana, M., 2005. Novel autoantibodies to a voltage-gated potassium channel Kv1.4 in a severe form of myasthenia gravis. J. Neuroimmunol. 170, 141–149.

Suzuki, S., Utsugisawa, K., Yoshikawa, H., Motomura, M., Matsubara, S., Yokoyama, K., Nagane, Y., Maruta, T., Satoh, T., Sato, H., Kuwana, M., Suzuki, N., 2009. Autoimmune targets of heart and skeletal muscles in myasthenia gravis. Arch. Neurol. 66, 1334–1338.

Todd, D.J., Lee, A.H., Glimcher, L.H., 2008. The endoplasmic reticulum stress response in immunity and autoimmunity. Nat. Rev. Immunol. 8, 663–674.

Turner, M.J., Delay, M.L., Bai, S., Klenk, E., Colbert, R.A., 2007. HLA-B27 up-regulation causes accumulation of misfolded heavy chains and correlates with the magnitude of the unfolded protein response in transgenic rats: implications for the pathogenesis of spondylarthritis-like disease. Arthritis Rheum. 56, 215–223.

Vattemi, G., Engel, W.K., McFerrin, J., Askanas, V., 2004. Endoplasmic reticulum stress and unfolded protein response in inclusion body myositis muscle. Am. J. Pathol. 164, 1–7.

Wiendl, H., Hohlfeld, R., Kieseier, B.C., 2005. Immunobiology of muscle: advances in understanding an immunological microenvironment. Trends Immunol. 26, 373–380.

Zhang, K., Kaufman, R.J., 2006. The unfolded protein response: a stress signaling pathway critical for health and disease. Neurology 66, S102–S109.

Desmoglein 3–specific CD4+ T cells induce pemphigus vulgaris and interface dermatitis in mice

Hayato Takahashi,[1] Michiyoshi Kouno,[1] Keisuke Nagao,[1] Naoko Wada,[1] Tsuyoshi Hata,[1] Shuhei Nishimoto,[1] Yoichiro Iwakura,[2] Akihiko Yoshimura,[3] Taketo Yamada,[4] Masataka Kuwana,[5] Hideki Fujii,[3] Shigeo Koyasu,[3] and Masayuki Amagai[1]

[1]Department of Dermatology, Keio University School of Medicine, Shinjuku-ku, Tokyo, Japan. [2]Center for Experimental Medicine and Systems Biology, Institute of Medical Science, University of Tokyo, Minato-ku, Tokyo, Japan. [3]Department of Microbiology and Immunology, [4]Department of Pathology, and [5]Division of Rheumatology, Department of Internal Medicine, Keio University School of Medicine, Shinjuku-ku, Tokyo, Japan.

Pemphigus vulgaris (PV) is a severe autoimmune disease involving blistering of the skin and mucous membranes. It is caused by autoantibodies against desmoglein 3 (Dsg3), an adhesion molecule critical for maintaining epithelial integrity in the skin, oral mucosa, and esophagus. Knowing the antigen targeted by the autoantibodies renders PV a valuable model of autoimmunity. Recently, a role for Dsg3-specific CD4+ T helper cells in autoantibody production was demonstrated in a mouse model of PV, but whether these cells exert cytotoxicity in the tissues is unclear. Here, we analyzed 3 Dsg3-specific TCRs using transgenic mice and retrovirus induction. Dsg3-specific transgenic (Dsg3H1) T cells underwent deletion in the presence of Dsg3 in vivo. Dsg3H1 T cells that developed in the absence of Dsg3 elicited a severe pemphigus-like phenotype when cotransferred into immunodeficient mice with B cells from *Dsg3*$^{-/-}$ mice. Strikingly, in addition to humoral responses, T cell infiltration of Dsg3-expressing tissues led to interface dermatitis, a distinct form of T cell–mediated autoimmunity that causes keratinocyte apoptosis and is seen in various inflammatory/autoimmune skin diseases, including paraneoplastic pemphigus. The use of retrovirally generated Dsg3-specific T cells revealed that interface dermatitis occurred in an IFN-γ– and TCR avidity–dependent manner. This model of autoimmunity demonstrates that T cells specific for a physiological skin-associated autoantigen are capable of inducing interface dermatitis and should provide a valuable tool for further exploring the immunopathophysiology of T cell–mediated skin diseases.

Introduction

Desmoglein 3 (Dsg3) is a cadherin-type glycoprotein expressed in stratified squamous epithelium, including the skin, oral mucosa, and esophagus, and it plays a critical role in cell-cell adhesion. Dsg3 is the IgG-targeted autoantigen in pemphigus vulgaris (PV) (1). Binding of anti-Dsg3 autoantibodies to epithelial cell surfaces in PV patients and PV model mice inhibits Dsg3 function and leads to the loss of cell-cell adhesion, which manifests clinically as skin blisters and erosions, and histologically as suprabasilar acantholysis (2–4). The antigen-specific autoimmunity in PV makes this disease a valuable model for studying not only autoreactive B cells, but also T cells. Given the importance of the helper function of CD4+ T cells in Ab production (5, 6), autoreactive CD4+ T cells are believed to play critical roles in the pathogenesis of PV. Recently, Dsg3-reactive CD4+ T cell clones were established from *Dsg3*$^{-/-}$ mice (7, 8). Some clones showed helper activity for anti-Dsg3 IgG production and induced the PV phenotype when adoptively transferred with *Dsg3*$^{-/-}$ B cells into *Rag2*$^{-/-}$ mice. Analysis of these clones demonstrated that IL-4 production was critical for Dsg3-reactive T cells in inducing anti-Dsg3 IgG production and the PV phenotype in vivo (7).

T cells are also involved in a rare subset of pemphigus called paraneoplastic pemphigus (PNP). PNP occurs in association with hematopoietic neoplasms and exhibits more complex features than PV (9–11). Anti-Dsg3 and -Dsg1 autoantibodies are detected in PNP, as are autoantibodies against the plakin family, including plectin, desmoplakin I and II, BP230, envoplakin, and periplakin. In addition to acantholysis caused by anti-Dsg3 and -Dsg1 autoantibodies (12), the coexistence of cellular infiltration into lesional epithelial tissue, known as interface dermatitis, is a characteristic histopathological feature in PNP (13). Interface dermatitis is a distinct histological condition in which epidermal basal cell damage occurs subsequent to inflammation at the dermal-epidermal junction. The inflammatory infiltrates consist predominantly of T lymphocytes, and the presence of apoptotic keratinocytes suggests T cell immunity against putative antigens displayed on the surfaces of keratinocytes. Interface dermatitis is observed not only in PNP, but also commonly in lichen planus (LP), lichen sclerosis (LS), toxic epidermal necrolysis/Stevens-Johnson syndrome (TEN/SJS), graft-versus-host disease (GVHD), lupus erythematosus, and other diseases (9, 14–17).

Despite the notion that these skin-infiltrating T cells are autoreactive in nature, there have been few studies of the target antigens, which remain largely unknown, because, unlike Abs, which recognize native proteins, T cell receptors recognize protein peptides in the context of class I or II MHCs. MHC polymorphism and the difficulty in preparing a screening library for peptide-MHC complexes have hampered progress in defining antigen specificity in T cells that infiltrate in inflammatory skin diseases. Consequently, it is unclear whether autoreactive T cells contribute to the pathogenesis of inflammatory skin diseases.

Authorship note: Hayato Takahashi and Michiyoshi Kouno contributed equally to this work.

Conflict of interest: The authors have declared that no conflict of interest exists.

Citation for this article: *J Clin Invest.* 2011;121(9):3677–3688. doi:10.1172/JCI57379.

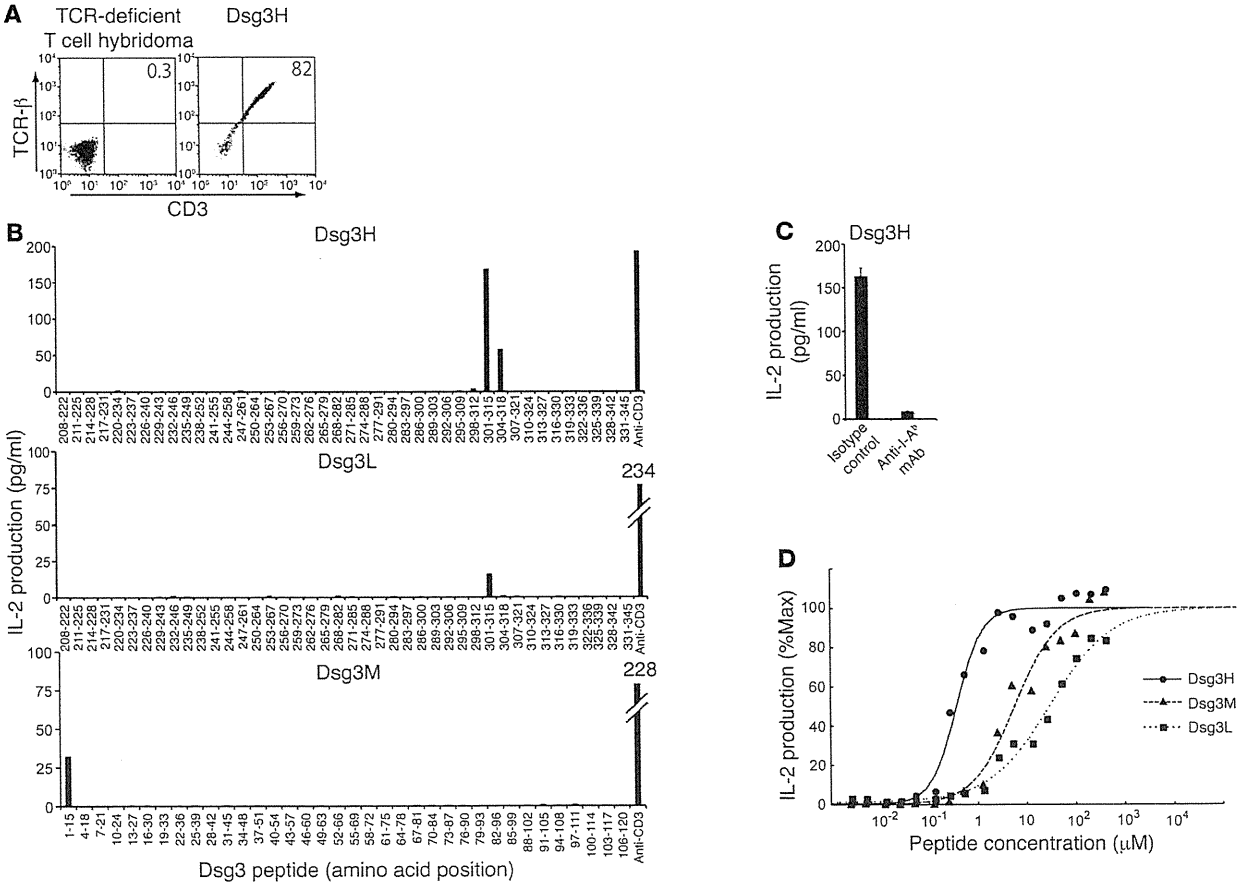

Figure 1

Identification of epitope peptides for 3 Dsg3-specific TCRs and a comparison of the differences in their avidities. (**A**) TCR-deficient T cell hybridoma was stably transfected by Dsg3H TCR-α and -β chain genes. Successful coexpression of TCR-β chain and CD3 molecules was subsequently detected by flow cytometry. (**B**) After the Dsg3H, Dsg3L, or Dsg3M hybridoma cell line was cultured with each Dsg3 peptide and irradiated splenocytes or stimulated by anti-CD3 Ab, IL-2 in the supernatant was quantified by ELISA. (**C**) The Dsg3H-transfectant was stimulated with peptide Dsg3(aa 301–315) in the presence or absence of anti-I-A^b Ab. Then, IL-2 was quantified by ELISA. (**D**) Dsg3H (line), Dsg3M (thick dotted line), and Dsg3L (fine dotted line) hybridoma cell lines were cultured with various concentrations of the corresponding peptide and irradiated splenocytes and the supernatant was subjected to IL-2 ELISA. Similar results were obtained in 2 separate experiments.

Here, we report the generation of transgenic mice in which T cells express Dsg3-specific TCRs. Dsg3-specific $CD4^+$ T cells that developed in the absence of Dsg3 caused severe mouse pemphigus when cotransferred with *Dsg3*$^{-/-}$ B cells into *Rag2*$^{-/-}$ mice. Of interest, histological examination of these mice revealed not only epidermal acantholysis (loss of keratinocyte adhesion), but also T cell infiltration of skin that exhibited interface dermatitis. Studies using WT T cells that were retrovirally transduced with Dsg3-specific TCRs revealed that T cells expressing different Dsg3-specific TCRs could induce interface dermatitis and that IFN-γ was a critical factor in inducing this phenotype.

Results

Cloning of 3 different TCR genes from Dsg3-reactive T cell clones. Several Dsg3-reactive T cell clones were previously established from lymph node cells of *Dsg3*$^{-/-}$ mice that were immunized with the extracellular domain of recombinant Dsg3 (7). cDNAs encoding the TCR-α and -β chains were obtained from 3 different T cell clones: 140#27 (AV8S13-J21 and BV6S1-XDX-Jβ1.3), 162#24 (AV20S1-J39 and BV8S1-XDX-Jβ2.7), and 164#2 (AV15S1-J45 and BV6S1-XDX-Jβ2.3). These were subcloned into cassette vectors to enable the expression of both the TCR-α and -β chains (Supplemental Table 1; supplemental material available online with this article; doi:10.1172/JCI57379DS1). The mRNA and amino acid sequences, including the CDR3 regions from these TCR-α and -β chains, are shown in Supplemental Figures 1–6.

Dsg3-specific TCRs recognize Dsg3 peptides with different avidities. Vectors constructed to express TCR from 140#27, 162#24, and 164#2 were introduced into TCR-deficient hybridoma cell lines by electroporation to generate Dsg3-specific T cell hybridoma cell lines, referred to as Dsg3H, Dsg3M, and Dsg3L, respectively. TCR-β chain and CD3 molecules were detected on the cell surface of the stable transfectants, indicating that the transduced TCR-α and -β chains were properly assembled on the cell surfaces as a complex with CD3 molecules (Figure 1A and other data not shown). Because the parental T cell clones 140#27 and 164#2 showed proliferative responses on stimulation with the recombinant Dsg3 extracellular domain (aa 210–345), and 162#24 to the Dsg3 extracellular domain (aa 1–119) (7), overlapping Dsg3 peptides covering aa 208–345 and aa 1–120 of

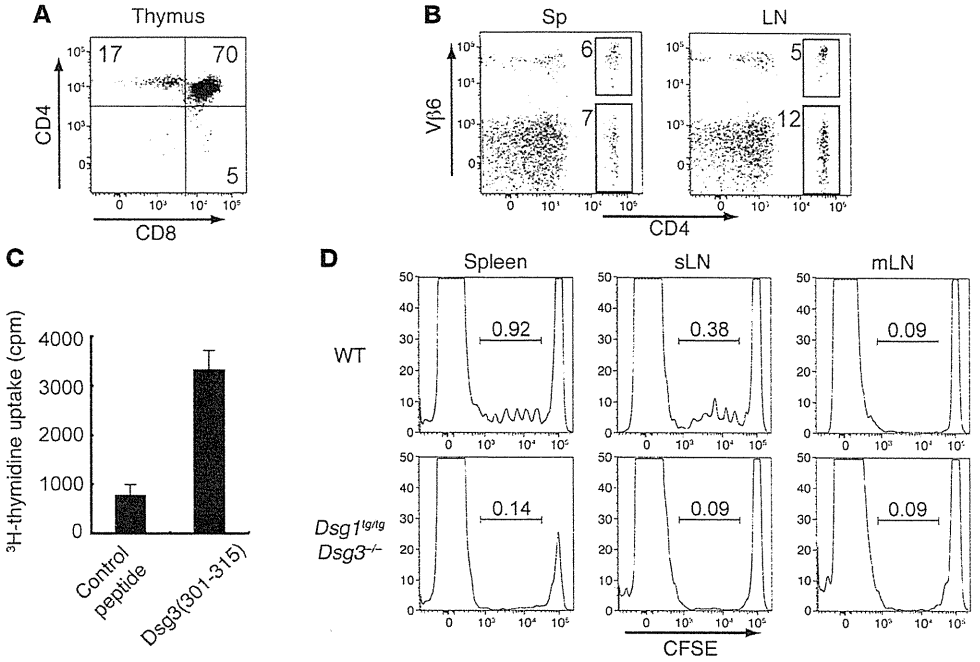

Figure 2

Generation of the Dsg3-specific TCR-transgenic mouse, Dsg3H1 mouse, and Dsg3 reactivity of transgenic T cells. (**A**) Thymocytes were stained with anti-CD4 and -CD8 Abs and analyzed by flow cytometry. (**B**) Single-cell suspensions from the spleen and LNs were stained with anti-CD4 and -Vβ6 Abs and analyzed. (**C**) Splenocytes from Dsg3H1 mice were cultured with the peptide Dsg3(aa 301–315) or a control peptide. ^{3}H-thymidine incorporation by these splenocytes is shown as the in vitro reactivity against Dsg3 peptide. (**D**) CFSE-labeled CD4$^+$ T cells from Dsg3H1 mice were transferred into B6 WT mice and *Dsg1$^{tg/tg}$Dsg3$^{-/-}$* mice. 3 days later, CFSE dilution was analyzed by flow cytometry after gating CD4$^+$Vβ6$^+$ cells of the spleen, skin-draining LN (sLN), and mesentery LN (mLN) from both recipients. Proportions of dividing cells were shown in each histogram. Similar results were obtained in 2 separate experiments. Data represent mean ± SEM.

Dsg3 were prepared to determine the epitopes for Dsg3H, Dsg3M, and Dsg3L TCR. The Dsg3H hybridoma cell line vigorously produced IL-2 when cocultured with irradiated splenocytes and the peptide Dsg3(aa 301–315), which has the sequence RNKAEFHQSVISQYR (Figure 1B). Interestingly, the Dsg3L hybridoma cell line also produced IL-2 on stimulation with Dsg3(aa 301–315), demonstrating that Dsg3H and Dsg3L recognize identical Dsg3 epitopes. The Dsg3M hybridoma cell line produced IL-2 on stimulation with Dsg3(aa 1–15), which has the sequence EWVKFAKPCREREDN, the endmost peptide of the N-terminus of the mature Dsg3 protein. The reactivity of Dsg3H, Dsg3M, and Dsg3L with the corresponding peptides was inhibited when cultured in the presence of anti–MHC class II blocking Ab (Figure 1C and other data not shown), demonstrating that these TCRs recognized Dsg3 peptides in an I-A^b–restricted manner. The synthetic peptides tested here may not necessarily be identical to the ones processed from the native Dsg3 protein. Nevertheless, these TCRs recognized Dsg3 peptides processed in vivo, suggesting that the synthetic peptide Dsg3(aa 301–315) is at least similar, if not identical, to a naturally processed peptide in vivo (Figure 2D). Although appropriate expression of the TCR-α chains of these 3 TCRs could not be confirmed using commercial anti-Vα Abs, this functional assay indicated that both the TCR-α and -β chains were properly expressed.

The avidity of each TCR complex was further evaluated by stimulation with various concentrations of antigenic peptides. All of the Dsg3-specific T cell hybridoma cell lines responded to the corresponding Dsg3 peptides in a dose-dependent manner (Figure 1D). Interestingly, Dsg3H TCR recognized the MHC peptide complex with greater avidity than Dsg3L TCR (ED_{50} 0.37 μM for Dsg3H and 29.3 μM for Dsg3L). Dsg3M TCR showed medium avidity, with an ED_{50} of 5.68 μM, and together with Dsg3H and Dsg3L, provided an interesting set of Dsg3-specific TCRs with differing levels of avidity, at least in the I-A^b background.

Generation of Dsg3-specific TCR-transgenic mice. The development of transgenic mice that express Dsg3-specific TCRs should enable a better understanding of the roles of autoreactive T cells in the pathogenesis of pemphigus in vivo. T cell clone 140#27 induced anti-Dsg3 Ab production and the PV phenotype in vivo when cotransferred with *Dsg3$^{-/-}$* B cells into *Rag2$^{-/-}$* mice (7). Thus, the TCR from this clone was used to generate TCR transgenic mice, Dsg3H mice. Ultimately, to be able to study the development of autoreactive T cells in detail, it was necessary to select a line of transgenic mice in which T cell development occurred in a manner comparable to that in WT mice. We chose the transgenic line Dsg3-specific transgenic (Dsg3H1) from among several lines because transgenic T cells in Dsg3H1 started to express the TCR-β chain at the DN4 stage in the thymus, as do WT αβ T cells under physiological conditions (Supplemental Figure 7). CD4 single-positive T cells developed in the thymuses of Dsg3H1 mice (Figure 2A). Of the CD4$^+$ population in the spleen and lymph nodes of the Dsg3H1 mouse, 30%–40% were Vβ6$^+$ cells (Figure 2B).

Transgenic CD4$^+$Vβ6$^+$ T cells from Dsg3H1 mice react to Dsg3. First, we examined the in vitro reactivity of CD4$^+$Vβ6$^+$ Dsg3H1 T cells to Dsg3. Splenocytes from Dsg3H1 mice were cultured with irradiated

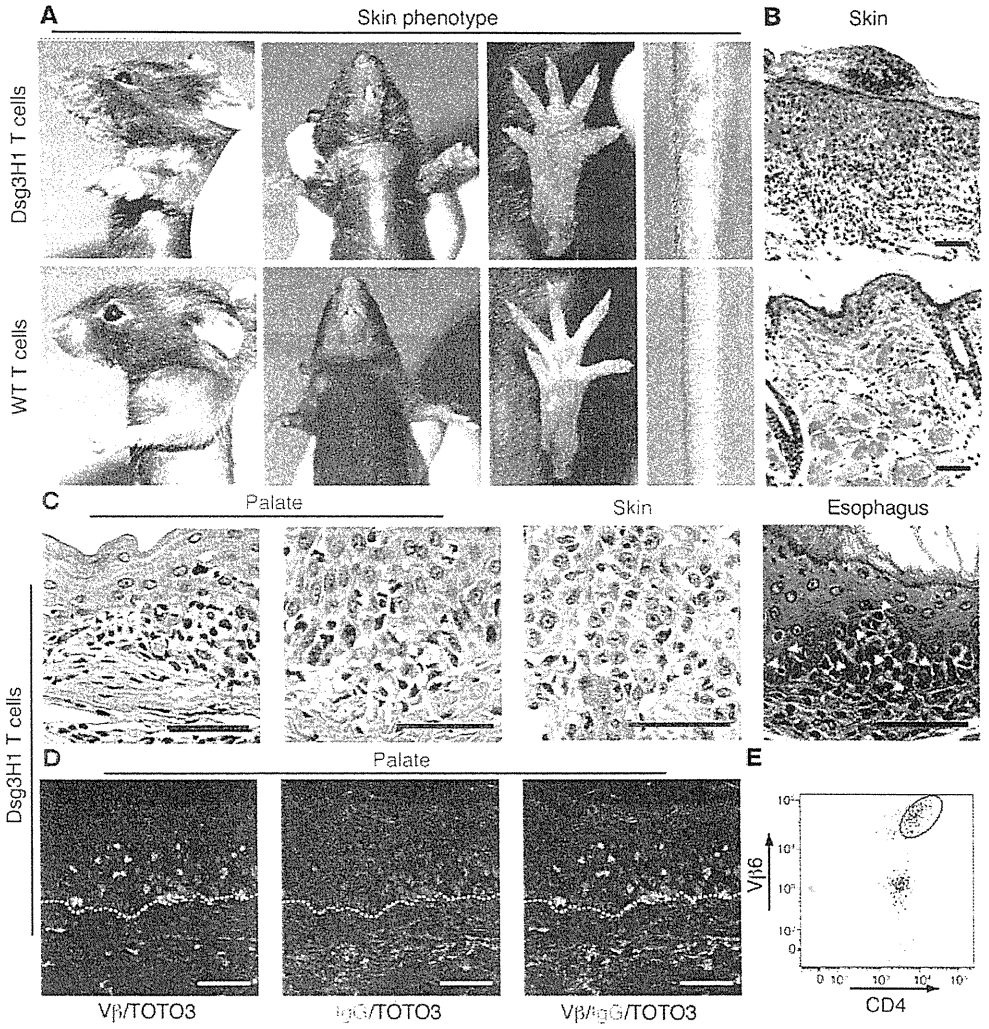

Figure 3

Tolerized Dsg3H1 T cells induced interface dermatitis, but not PV. (**A**) The skin phenotype of *Rag2*$^{-/-}$ mice (n = 3 per group) given CD4$^+$Vβ6$^+$ cells from Dsg3H1 mice or CD4$^+$ T cells from C57BL/6 mice in combination with *Dsg3*$^{-/-}$ B cells. Erosive and crusted lesion in the perioral region, upper limbs, paws, and tail and hair loss on the chest were evident (upper panels). (**B**) Pathology of the skin in the recipients given CD4$^+$Vβ6$^+$ cells from Dsg3H1 mice or WT CD4$^+$ T cells. (**C**) Various Dsg3-expressing tissues in the recipients of CD4$^+$Vβ6$^+$ cells from Dsg3H1 mice were stained with H&E. Blue arrowheads indicate degenerated cells in the epithelium. Yellow arrowheads indicate intraepithelial inflammatory cells. Blue arrows indicate liquefaction degeneration in the basal layer of the lesional epithelium. Yellow arrow indicates a degenerated cell well stained with eosin, a so-called Civatte body. (**D**) The palate was stained with anti–TCR-β chain (red) and anti-IgG (green) Abs and TOTO3 (blue). Dotted lines indicate the basement membrane zone. (**E**) A single-cell suspension was prepared from the lesional skin of the recipients given CD4$^+$Vβ6$^+$ cells from Dsg3H1 mice and analyzed by flow cytometry after gating into the CD45$^+$7-AAD$^-$ population. Scale bars: 50 μm.

splenocytes in the presence of the peptide Dsg3(aa 301–315), and their proliferation was analyzed using a ^{3}H-thymidine uptake assay. Addition of Dsg3 peptide induced proliferative responses, demonstrating that splenocytes from Dsg3H1 mice contained T cells that were functionally reactive to Dsg3(aa 301–315) ex vivo (Figure 2C).

We confirmed the antigen specificity of Dsg3H1 T cells in vivo. Because APCs present various antigenic peptides, including self antigens in the context of MHC class II molecules (18, 19), we evaluated whether APCs from WT mice were able to stimulate the proliferation of CD4$^+$ Dsg3H1 T cells in vivo. CD4$^+$ Dsg3H1 T cells were labeled with CFSE and then adoptively transferred into C57BL/6 WT mice or *Dsg1*$^{tg/tg}$*Dsg3*$^{-/-}$ C57BL/6 mice. *Dsg1*$^{tg/tg}$*Dsg3*$^{-/-}$ mice express Dsg1, driven by the keratin 5 promoter, which functionally compensates for the loss of Dsg3, leading to better survival in various experimental settings (20). Three days after the transfer, CFSE dilution of CD4$^+$Vβ6$^+$ cells was detected in both the spleen and skin-draining LNs, but not in the mesenteric LNs of C57BL/6 WT mice. Importantly, no CFSE dilution was detected in any of the *Dsg1*$^{tg/tg}$*Dsg3*$^{-/-}$ mice, indicating that CD4$^+$ Dsg3H1 T cells proliferated only in the presence of Dsg3, further ensuring the antigen reactivity of these cells in vivo (Figure 2D).

Transgenic Dsg3H1 T cells undergo Dsg3-dependent T cell selection. Despite the forced expression of Dsg3-specific TCR, only 30%–40% of the CD4$^+$ T cells were Vβ6$^+$ in Dsg3H1 mice. Conceivably, the rel-

Table 1
Dsg3-specific TCRs and their abilities to induce interface dermatitis in the recipient mice after adoptive transfer of Dsg3-specific T cells with *Dsg3*$^{-/-}$ B cells into *Rag2*$^{-/-}$ mice

Dsg3-specific TCR, epitope, avidity	T cell source	
	TCR transgenic mouse	Retroviral transduction
Dsg3H, Dsg3(aa 301–315), high	+	+
Dsg3M, Dsg3(aa 1–15), medium	ND	+
Dsg3L, Dsg3(aa 301–315), low	–	–

ND, not determined.

atively low number of Vβ6$^+$ cells is due to the presence of tolerance mechanisms in these Dsg3-expressing animals. To determine the effect of the presence or absence of Dsg3 during T cell development, BM cells from Dsg3H1 mice (Ly9.2, I-A^b) were transferred into sublethally irradiated 129/Sv WT and 129/Sv *Dsg3*$^{-/-}$ mice (Ly9.1, I-A^b) to generate BM chimeric mice, referred to as Dsg3H1→WT mice and Dsg3H1→*Dsg3*$^{-/-}$ mice, respectively (Supplemental Figure 8). Because of the sublethal irradiation dose, efficient adaptation of the donor BM occurs in the presence of recipient hematopoietic cells that are not eradicated by irradiation, allowing the evaluation of Dsg3H1 T cell development as a subpopulation among a diverse repertoire of T cells. The donor Ly9.2$^+$ T cells can be distinguished from recipient Ly9.1$^+$ T cells using an anti-Ly9.1 Ab. Strikingly, in Dsg3H1→*Dsg3*$^{-/-}$ mice, in which Dsg3H1 T cells developed in the absence of Dsg3, Ly9.1$^-$CD4$^+$ Vβ6$^+$ cells constituted over 95% of the donor-derived CD4$^+$ T cells. Under the *Dsg3*$^{+/+}$ condition in Dsg3H1→WT mice, the proportion of Ly9.1$^-$CD4$^+$ Vβ6$^+$ T cells was much decreased, to proportions similar to those of Dsg3H1 mice (Supplemental Figure 9A). These results demonstrated that T cell tolerance mechanisms against Dsg3 exist in WT mice and that Dsg3H1 T cells undergo Dsg3-dependent negative selection in Dsg3H1 mice. However, the incomplete deletion may reflect Dsg3H1 T cells that had "escaped" from the deletion process.

Tolerance mechanisms inhibit the induction of PV, but not interface dermatitis, by Dsg3H1 T cells. We questioned whether the Dsg3-reactive CD4$^+$Vβ6$^+$ T cells that were present in the periphery of Dsg3H1 mice, which presumably had escaped the above-described tolerance mechanisms, still had the capacity to induce PV. To determine this, Dsg3H1 T cells were isolated from Dsg3H1 mice directly and cotransferred with *Dsg3*$^{-/-}$ B cells into *Rag2*$^{-/-}$ mice. Fine scales and mild erythema developed on the ears, neck, tail, and soles within 1 week of adoptive transfer; these progressed to erosions and swelling of the arms, perioral region, and trunk (Figure 3A). This phenotype was not observed in the recipients that were cotransferred with simultaneously isolated WT CD4$^+$ T cells and *Dsg3*$^{-/-}$ B cells.

Strikingly, however, no anti-Dsg3 IgG Abs were found in serum from these mice (data not shown). Histopathological studies revealed massive inflammatory cell infiltrates not only in skin, but also in the palate and esophagus, the epithelia of which express Dsg3 (Figure 3, B and C, and Supplemental Figure 10). Lesional epithelia exhibited acanthosis and hyperkeratosis, and keratinocytes undergoing apoptosis and degeneration were observed among the infiltrating lymphocytes. Liquefaction degeneration was observed in the basal cell layers (Figure 3C), where apoptotic keratinocytes resembled Civatte bodies (Figure 3C), as seen in human diseases that involve interface dermatitis (21, 22). These features indeed fulfilled the criteria of human interface dermatitis (Table 1). Immunofluorescence microscopy revealed the infiltration of TCR-β$^+$ T cells in the epidermis (Figure 3D), and a major population of these was identified as CD4$^+$Vβ6$^+$ T cells by flow cytometry (Figure 3E). In contrast with the lymphocyte infiltration, neither suprabasilar acantholysis nor IgG deposition on the surface of keratinocytes was detected (Figure 3, C and D), consistent with the absence of anti-Dsg3 IgG Abs in serum from these mice. Thus, Dsg3H1 T cells that had developed in the presence of Dsg3 did not exert helper activity for B cell autoantibody production to cause PV, but were capable of inducing interface dermatitis, a distinct T cell–mediated inflammation at the dermal-epidermal junction seen in LP, LS, lupus, GVHD, SJS/TEN, PNP, and other diseases.

Nontolerized Dsg3H1 T cells induce both anti-Dsg3 IgG production and interface dermatitis. Paradoxically, whereas the parental T cell clone of Dsg3H1 TCR, 140#27, helped *Dsg3*$^{-/-}$ B cells to produce anti-Dsg3 autoantibodies, Dsg3H1 T cells could not. We next asked whether the presence or absence of Dsg3 during T cell development influenced the fate of T cell development in Dsg3H1 mice. 140#27 was originally established from *Dsg3*$^{-/-}$ mice (7). Thus, to mimic this developmental setting, the pathogenic activity of transgenic Dsg3H1 T cells was evaluated using BM chimeric Dsg3H1→*Dsg3*$^{-/-}$ mice. Ly9.1$^-$CD4$^+$ T cells in Dsg3H1→*Dsg3*$^{-/-}$ mice, referred to as Dsg3H1→*Dsg3*$^{-/-}$ CD4$^+$ T cells, showed the CD44^{lo} naive T cell phenotype and expressed the Vβ6 chain (Supplemental Figure 9, A and B). These naive Dsg3H1→*Dsg3*$^{-/-}$ CD4$^+$ T cells were isolated and cotransferred with *Dsg3*$^{-/-}$ B cells into *Rag2*$^{-/-}$ mice (Supplemental Figure 8) and were analyzed 1 week after adoptive transfer. Ly9.1$^-$CD4$^+$ T cells in Dsg3H1→WT mice, referred to as Dsg3H1→WT CD4$^+$ T cells, were used as a control. Because Dsg3H1→WT CD4$^+$ T cells contained approximately 30% of the CD44^{hi} population (memory/activated phenotype; Supplemental Figure 9B), naive T cells were isolated by depleting CD44^{hi} memory cells from the Ly9.1$^-$CD4$^+$ cell population of Dsg3H1→WT mice (Supplemental Figure 9B) and transferred with *Dsg3*$^{-/-}$ B cells into *Rag2*$^{-/-}$ mice (Supplemental Figure 8). The recipient mice that received naive Dsg3H1→*Dsg3*$^{-/-}$ CD4$^+$ T cells and *Dsg3*$^{-/-}$ B cells developed erythma and crusted lesion on the trunk, neck, limbs, face, and paws (Figure 4A). ELISA showed that anti-Dsg3 IgG was produced in these recipient mice (Figure 4B). Living cell staining also demonstrated that IgG from these mice bound to native antigens expressed on the surfaces of the mouse epidermal cell line (Pam cells) (Figure 4C). Consistently, histopathological analysis revealed suprabasilar acantholysis in the palate (Figure 4D). In addition to suprabasilar acantholysis, however, CD4$^+$ T cell infiltration of the epithelium and lamina propria mucosae was observed in the palate. Immunofluorescence analysis demonstrated the coexistence of IgG deposition on the epithelial cell surfaces and Vβ$^+$ T cell infiltration (Figure 4E and Table 2). There were no detectable circulating IgG Abs against desmoplakin, envoplakin, and periplakin in the recipient mice (data not shown). The combination of suprabasilar acantholysis and interface dermatitis observed in this mouse model is similar to the pathological changes observed in human PNP (Figure 4F).

In contrast, anti-Dsg3 IgG was not detected in the recipient mice transferred with naive Dsg3H1→WT CD4$^+$ T cells and *Dsg3*$^{-/-}$ B cells by either ELISA, living cell staining, or immunofluorescence analyses (Figure 4, B, C, and E), and suprabasilar acantholysis by histology was not observed in the palate (Figure 4D). However,

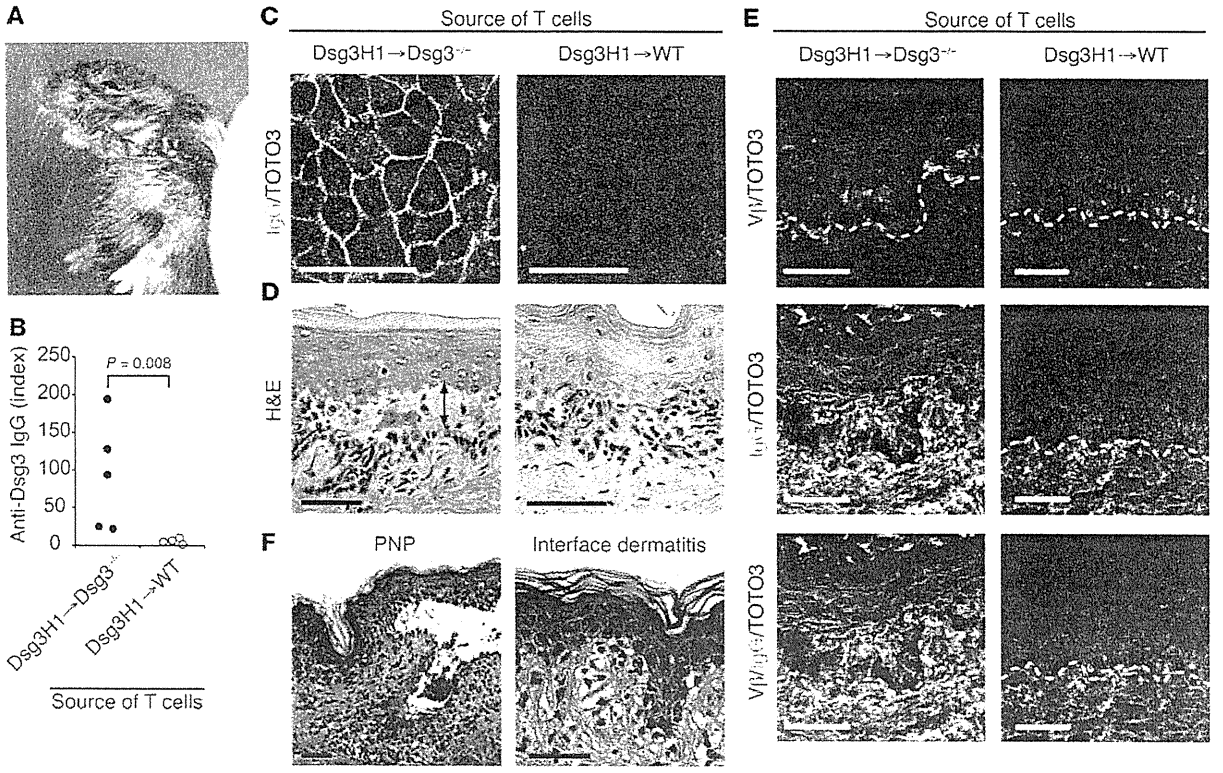

Figure 4

Nontolerized Dsg3H1 T cells induce both anti-Dsg3 IgG production and interface dermatitis. BM cells from Dsg3H1 mice (Ly9.2) were transferred into sublethally irradiated 129/Sv WT and *Dsg3*$^{-/-}$ mice (Ly9.1) to generate BM chimeric mice, referred to as Dsg3H1→WT and Dsg3H1→*Dsg3*$^{-/-}$ mice, respectively. Donor-derived naive CD4^{+}Vβ6^{+}CD44^{-}Ly9.1^{-} cells were enriched from Dsg3H1→WT and Dsg3H1→*Dsg3*$^{-/-}$ mice and were cotransferred with *Dsg3*$^{-/-}$ B cells into *Rag2*$^{-/-}$ mice. (**A**) Skin phenotype in the recipient mice that received donor-derived CD4^{+} T cells from Dsg3H1→*Dsg3*$^{-/-}$ mice and *Dsg3*$^{-/-}$ B cells. Erythema and crusted lesions were observed in face, neck, and limbs. (**B**) Anti-Dsg3 IgG Ab titers in sera from the recipients were analyzed by ELISA. Statistical analysis was performed using the Mann-Whitney *U* test. (**C**) Sera from the recipients were added to the culture medium of Pam cells. IgG deposition on the cell surfaces was subsequently detected by anti-IgG Ab Alexa Fluor 488. Nuclei were stained with TOTO3 (blue). (**D**) Palates of the recipients were analyzed by H&E staining. The arrow indicates suprabasilar acantholysis. (**E**) Intraepidermal T cells (red) and IgG deposition (green) in the recipient's palate were detected using anti–TCR-β Ab and anti-mouse IgG Ab, respectively. Dotted lines show the basement membrane zone. Similar results were obtained in 2 separate experiments. (**F**) The skin histopathology of PNP and interface dermatitis (GVHD) are shown. Scale bars: 50 μm.

some cell infiltration was observed in the palate of the recipient with naive Dsg3H1→WT CD4^{+} T cells, and immunofluorescence analysis identified the infiltrating cells as Vβ^{+} cells (Figure 4E and Table 2). Similar infiltration was observed in the skin and esophagus, where Dsg3 was expressed (data not shown). These results demonstrated that nontolerized Dsg3-specific CD4^{+} T cells that developed in the absence of Dsg3 are able not only to induce suprabasilar acantholysis via the production of anti-Dsg3 autoantibodies, but are also capable of infiltrating skin directly to cause interface dermatitis, which in combination, showed some findings that are seen in PNP. These results suggest that those Dsg3H1 T cells that are capable of inducing PV are highly reactive with Dsg3 and are negatively selected in the *Dsg3*$^{+/+}$ environment.

Avidity-dependent induction of interface dermatitis by Dsg3-specific T cells. Because we had cloned 3 different Dsg3-specific TCRs with differing avidities, this gave us an opportunity to determine whether different TCRs specific for Dsg3 could induce interface dermatitis and to evaluate any relationship between TCR avidity and clinical severity. To determine this, we retrovirally transduced WT CD4^{+} T cells with Dsg3-specific TCRs Dsg3H, Dsg3M, or Dsg3L, each with differing avidities for Dsg3 (see Figure 1D). By performing transduction on WT CD4^{+} T cells, it is possible to circumvent TCR avidity–specific events that may occur during thymic selection. WT CD4^{+} T cells were retrovirally transduced with Dsg3H TCR to generate rvDsg3H T cells, which properly acquired Dsg3 reactivity, shown by the robust IL-2 production on stimulation with Dsg3(aa 301–315) (Supplemental Figure 11). When rvDsg3H T cells were transferred with or without *Dsg3*$^{-/-}$ B cells into *Rag2*$^{-/-}$ mice, the recipient mice developed erosive and crusted lesions on the ears, neck, periorbital region, paws, and tail (Figure 5A). Histopathological analysis revealed interface dermatitis in the skin, palate, and esophagus (Figure 5A and other data not shown). Interface dermatitis was not observed in non–Dsg3-expressing tissues, including the liver and small and large intestines (Supplemental Figure 12). Furthermore, recipients to which *Dsg3*$^{-/-}$ B cells were also transferred showed no anti-Dsg3 IgG production or PV phenotype (Supplemental Figure 13). Control animals that received CD4^{+} T cells transduced with control retro-

Table 2
Phenotype of the recipient mice after adoptive transfer of BM chimera-derived Dsg3H1 cells with *Dsg3*$^{-/-}$ B cells into *Rag2*$^{-/-}$ mice

	BM chimera as T cell source	
Phenotype	**Dsg3H1→WT**	**Dsg3H1→*Dsg3*$^{-/-}$**
IgG production[A], acantholysis	–	+
Interface dermatitis	+	+

[A]Dsg3-specific Ab.

virus, rvGFP T cells, did not develop any phenotype (Figure 5A). Overall, the phenotype induced by rvDsg3H T cells was nearly identical to that of Dsg3H1 T cells.

Next, we generated rvDsg3M (medium avidity) and rvDsg3L (low avidity) T cells, and transferred them into *Rag2*$^{-/-}$ mice with no B cells. Whereas mice that received rvDsg3M subsequently developed scaly erythema, comparable to mice that received rvDsg3H, mice that received rvDsg3L T cells did not develop any skin abnormalities (Figure 5, B and C). The histopathology of the lesional skin induced by rvDsg3H and rvDsg3M revealed interface dermatitis (Table 1). Consistent with earlier experiments, no lesion was seen in non–Dsg3-expressing tissues (Supplemental Figure 12).

To confirm the nonpathogenic nature of Dsg3L TCR in inducing interface dermatitis, a Dsg3L TCR transgenic mouse (i.e., the Dsg3L3 mouse) was evaluated. More than 90% of the CD4$^+$ T cells expressed Vβ6 in the spleen and LNs of Dsg3L3 mice (Supplemental Figure 14A). CD4$^+$Vβ6$^+$ T cells from Dsg3L3 transgenic mice were cotransferred with *Dsg3*$^{-/-}$ B cells into *Rag2*$^{-/-}$ mice, but unlike those that received Dsg3H1 T cells, the Dsg3L3 recipient mice did not develop any abnormalities, consistent with the results obtained with the retroviral system (Table 1 and Supplemental Figure 14B).

Thus, T cells expressing Dsg3-specific TCRs with high and medium avidity, but not those with low avidity, were capable of eliciting interface dermatitis. These results collectively demonstrated that interface dermatitis could be induced in an antigen-specific and a TCR avidity–dependent manner by Dsg3-specific CD4$^+$ T cells.

IFN-γ–dependent induction of interface dermatitis by Dsg3-specific T cells. To further understand the molecular events that influenced Dsg3H1 T cells to elicit different phenotypes depending on their exposure to Dsg3 during developmental processes, cytokine analyses were performed to clarify which T helper subset the Dsg3H1 T cells had differentiated into in vivo. Naive Dsg3H1 T cells that were cotransferred with *Dsg3*$^{-/-}$ B cells into *Rag2*$^{-/-}$ mice were isolated ex vivo after disease elicitation and were analyzed for IFN-γ, IL-4, IL-17A, and Foxp3. Dsg3H1→*Dsg3*$^{-/-}$ CD4$^+$ T cells and Dsg3H1→WT CD4$^+$ T cells were compared (Supplemental Figure 8) because these T cells induced both autoantibody production and interface dermatitis, or only interface dermatitis, respectively (Table 2).

Whereas IFN-γ was the predominant cytokine produced by Dsg3H1 T cells (Ly9.1$^-$CD4$^+$Vβ6$^+$) isolated from the spleens and LNs of both groups, Dsg3H1 T cells isolated from the skin-draining LNs of Dsg3H1→*Dsg3*$^{-/-}$ mice deviated more toward IL-4 production and expressed relatively lower levels of IFN-γ (Figure 6A). Interestingly, whereas a fraction of Dsg3H1→WT CD4$^+$ T cells had differentiated into IL-17A–expressing T cells, this was not observed in Dsg3H1→*Dsg3*$^{-/-}$ CD4$^+$ T cells (Figure 6B). Foxp3-expressing Dsg3H1 T cells were found in similar ratios in the spleen and skin-draining LNs from both groups. It seems likely that the presence or absence of an autoantigen influences T cell development and diversifies T cell properties, such as antigen reactivity, leading to striking differences in cytokine deviation and phenotypic outputs.

It caught our strong interest that in settings where interface dermatitis was the predominant phenotype, both IFN-γ– and IL-17A–producing Dsg3H1 T cells were detected, suggesting that these cytokines played important roles in interface dermatitis. To determine this, we took advantage of the retroviral expressing system, and CD4$^+$ T cells isolated from *Ifng*$^{-/-}$ and *Il17a*$^{-/-}$ mice were transduced to generate *Ifng*$^{-/-}$ or *Il17a*$^{-/-}$ rvDsg3H T cells. Within 3 weeks after the adoptive transfer of WT rvDsg3H T cells and *Il17a*$^{-/-}$ rvDsg3H T cells, *Rag2*$^{-/-}$ mice exhibited skin inflammation, showing scale, crusts, and erythema. Strikingly, however, *Ifng*$^{-/-}$ rvDsg3H T cells failed to elicit any abnormalities (Figure 6C). The histopathology of the skin lesions elicited by WT and *Il17a*$^{-/-}$ rvDsg3H T cells revealed typical interface dermatitis, while the skin of mice transferred with *Ifng*$^{-/-}$ rvDsg3H T cells showed no inflammatory infiltrate (Figure 6D). These findings demonstrated that IFN-γ, but not IL-17A, is the key cytokine produced by Dsg3-specific T cells that causes interface dermatitis.

Discussion

We generated Dsg3-specific TCR transgenic mice to analyze the development and roles of autoreactive CD4$^+$ T cells in PV. Bone marrow transplantation experiments demonstrated Dsg3 tolerance mechanisms in vivo. When Dsg3H1 T cells that developed in the absence of Dsg3 were cotransferred with *Dsg3*$^{-/-}$ B cells into *Rag2*$^{-/-}$ mice, these mice developed a severe skin phenotype mimicking PNP. Unexpectedly, in addition to Ab production by B cells, direct infiltration of Dsg3H1 T cells was seen in the skin, resulting in histological features that recapitulated interface dermatitis, a phenomenon that is not seen in PV, but in PNP. Retrovirally generated Dsg3H T cells showed that interface dermatitis could be induced independently of B cells, in an IFN-γ– and TCR avidity–dependent manner, indicating that autoimmunity by CD4$^+$ T cells directed against a defined physiological epidermal antigen is sufficient to cause interface dermatitis.

Interface dermatitis exhibits degenerative changes at the dermal-epidermal junction that are accompanied by lymphocytic infiltration (22). Interface dermatitis is divided into 2 subtypes: vacuolar type and lichenoid type (lichenoid dermatitis). Vacuolar types shows small vacuolar spaces at the dermal-epidermal junction, often leaving the junction indistinct. Leukocyte infiltration in this type may not be prominent. On the other hand, lichenoid types show a dense, band-like infiltrate of inflammatory cells, which consists mostly of lymphocytes, in the superficial dermis. Histological findings observed in the skin lesions of our model mice showed interface dermatitis with lymphocytic infiltrations that were not as dense as the band-like infiltration of the lichenoid type and thus more resembled the vacuolar type interface dermatitis, which is found in the original histological description for patients with PNP (9).

Interface dermatitis is observed in various inflammatory conditions of the skin and mucous membranes, including LP, LS, TEN/SJS, GVHD, lupus, and PNP. The infiltrating lymphocytes in LP lesions have been reported to be a mixture of CD4$^+$ and CD8$^+$ T cells (23), which appear, at least histologically, to "attack" the epidermal keratinocytes, causing apoptosis and obscuring the dermal-epidermal junction. It has been described that cytotoxic CD8$^+$ T cells are capable of directly injuring keratinocytes and thus play a central role in interface dermatitis (24, 25). Although there are very few reports that have studied the role of CD4$^+$ T cells in interface dermatitis, one study has

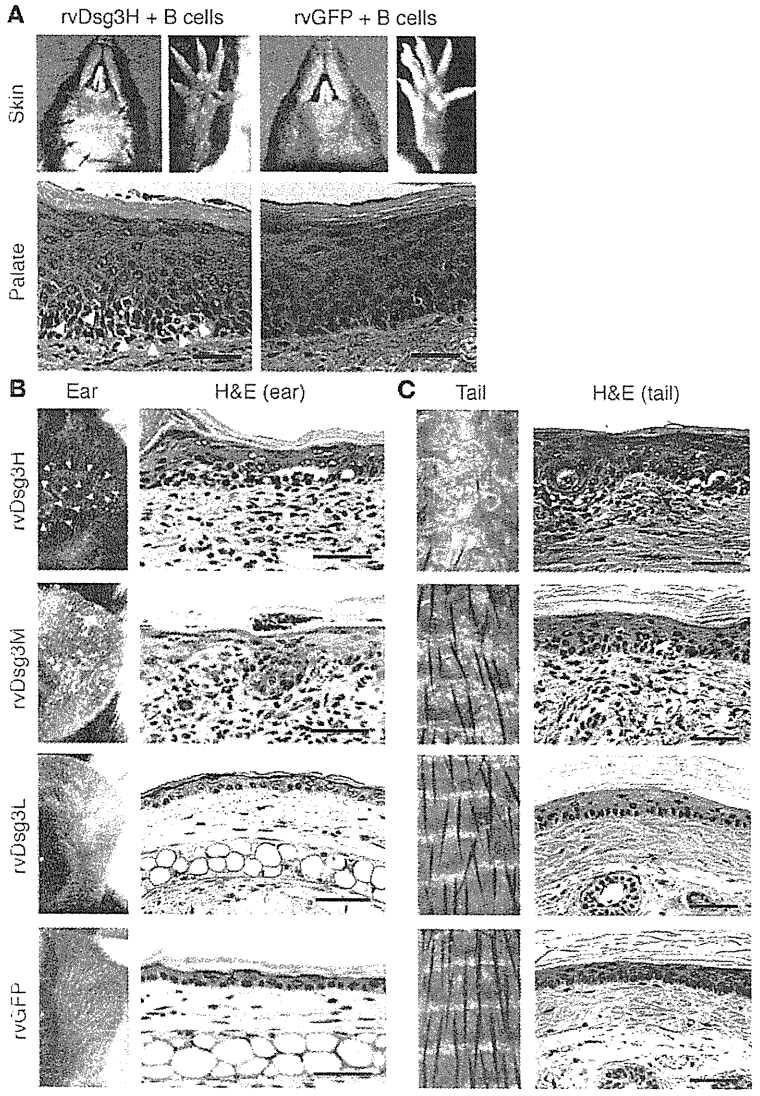

Figure 5

Avidity-dependent induction of interface dermatitis by retrovirally transduced Dsg3-specific T cells. Dsg3-specific T cells, including rvDsg3H, rvDsg3M, and rvDsg3L T cells, were generated by retroviral transduction of Dsg3H, Dsg3M, and Dsg3L TCRs into WT CD4$^+$ T cells, respectively. Control T cells, rvGFP T cells, were generated using control retrovirus. (**A**) The skin phenotype and histopathology of the palate from the recipient mice given rvDsg3H T cells and rvGFP T cells in combination with *Dsg3*$^{-/-}$ B cells. Blue arrows show erosive and crusted lesions. Yellow arrowheads indicate inflammatory cell infiltration. (**B** and **C**) rvDsg3H, rvDsg3M, rvDsg3L, and rvGFP T cells were transferred into *Rag2*$^{-/-}$ mice. 4 weeks later, the skin phenotype and histopathology of the ears (**B**) and tails (**C**) were observed. White arrowheads indicate a crusted lesion. Blue arrowheads indicate scaly lesions. Scale bars: 50 μm. Similar results were obtained from 2 independent experiments.

clearly demonstrated that CD4$^+$ T cells alone can injure keratinocytes (26). The cytotoxic effector function of CD4$^+$ T cells has been observed in other animal models, including EAE, with results that are also consistent with ours in terms of tissue injury by CD4$^+$ T cells (27). However, more fundamental questions, such as which population of T cells plays the initial role in triggering interface dermatitis and what proportion of infiltrating CD4$^+$ and CD8$^+$ T cells are specific to certain antigens in skin, remain unresolved. Thus, our experimental autoimmune dermatitis (EAD) model described in this study will provide a valuable tool to clarify such unsolved pathophysiological mechanisms of T cell–mediated skin diseases.

Despite the long-standing notion that these lymphocytes might recognize skin-associated autoantigens, strong evidence for autoimmunity and putative autoantigens is lacking. Interestingly, however, in LS and LP, both of which exhibit interface dermatitis, autoantibodies against extracellular matrix protein 1 (28) and type XVII collagen (29) have been reported, suggesting the existence of autoimmunity in these patients, further implying the possibility that skin-infiltrating T cells might also recognize the same autoantigen. CD8$^+$ T cell lines established from the lesional skin of LP patients exerted cytotoxic activity against immortalized autologous keratinocytes, supporting the involvement of skin-targeted autoimmunity in the development of interface dermatitis (30).

Likewise, the autoantibody targets in PNP are well characterized, but the relative importance of T cell immunity in the pathology and nature of the autoantigen were unclear. The dermatitis observed in our EAD model is a CD4$^+$ T cell response. Thus, it does not fully recapitulate the immunity seen in PNP, in which Ab targets are not restricted to Dsg3, and CD8$^+$ T cells also contribute to the pathogenesis. Nevertheless, mice that were cotransferred with Dsg3H1 T cells and *Dsg3*$^{-/-}$ B cells exhibited PNP-like clinical and pathological features, including both acantholysis and interface dermatitis, resulting in a rapidly progressive course with high mortality. The coexistence of humoral immunity against Dsg3 and interface dermatitis is a phenotypic combination unique to PNP. The results of our murine study imply, for what we believe is the first time, that T cell immunity against Dsg3, among other targets, might exist in human PNP. The finding that direct tissue infiltration of T cells that recognize a specific skin-associated antigen leads to interface dermatitis extends its significance not only to Dsg3 and PV or PNP, but also to other diseases that display interface dermatitis and provides impetus for the further characterization of T cell–mediated inflammatory skin diseases.

Recent research has revealed new subsets of helper T cells and critical cytokines that induce specific responses, including autoimmunity. Th1 and Th17 differentiation and cytokines that support the development of helper T cell subsets, such as IL-12 and IL-23, have been investigated intensively in the context of autoimmune disease models. Th17 cells are important for disease development in collagen-induced arthritis (31–35). In contrast, Th1 cells have been reported to be critical for autoimmune diabetes (36–38). Furthermore, in EAE, conflicting results have been reported and the central role of a particular T helper subset in the induction of EAE is controversial (39–41). This evidence emphasizes that each autoimmune disease may involve differing mechanisms and the pathological mechanisms of each disease must be investigated carefully.

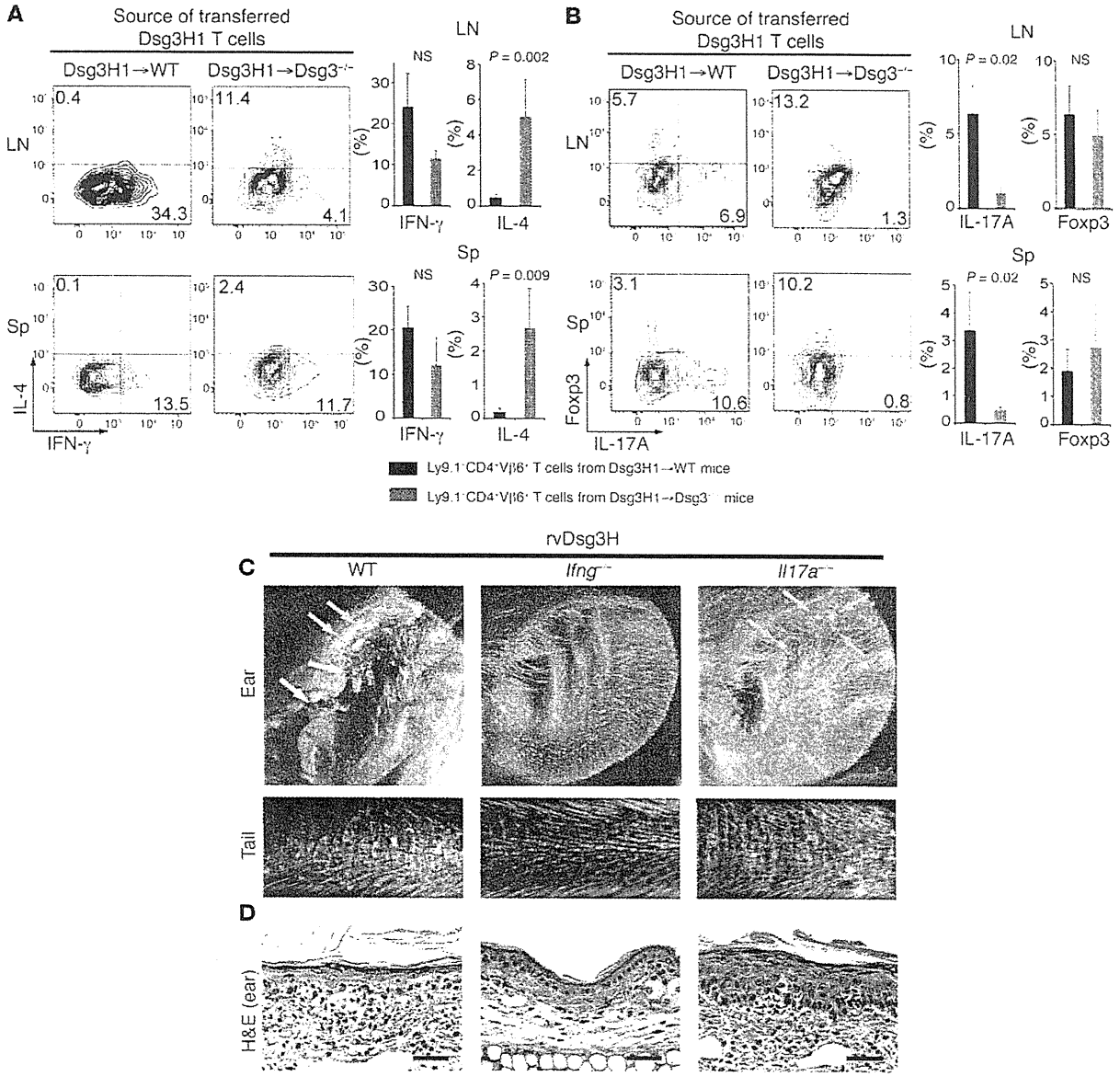

Figure 6

Dsg3-specific T cells induce interface dermatitis in an IFN-γ–dependent manner. (**A** and **B**) Naive Dsg3H1→WT or Dsg3H1→*Dsg3*$^{-/-}$ CD4$^+$ T cells were transferred with *Dsg3*$^{-/-}$ B cells into *Rag2*$^{-/-}$ mice. More than 6 days later, LN and spleen were collected and used to make a single-cell suspension, which was then treated with PMA, ionomycin, and brefeldin A, and flow cytometric analysis examined the expression of IFN-γ versus IL-4 (**A**) and IL-17A versus Foxp3 (**B**). Representative contour plots are shown after gating into the CD4$^+$Vβ6$^+$7-AAD$^-$ population. The quadrants were set based on the results of staining with isotype control Abs. Black bars represent the average for Ly9.1$^-$CD4$^+$Vβ6$^+$ T cells from Dsg3H1→WT mice (n = 6). Gray bars represent the average for Ly9.1$^-$CD4$^+$Vβ6$^+$ T cells from Dsg3H1→*Dsg3*$^{-/-}$ mice (n = 6). Error bars indicate the SEM. Statistical comparison was made using the Mann-Whitney U test. (**C** and **D**) CD4$^+$ T cells were isolated from WT, *Ifng*$^{-/-}$, or *Il17a*$^{-/-}$ mice and retrovirally transduced with Dsg3H TCR and transferred into *Rag2*$^{-/-}$ mice. 3 weeks later, the macroscopic phenotype (**C**) and histopathology of the skin (**D**) were observed. Yellow arrows indicate crusted lesions in the ear. Blue arrows indicate scaly lesions. Scale bars: 50 μm. Similar results were obtained from 2 independent experiments.

In our EAD model, the importance of IFN-γ, but not IL-17A, was clearly demonstrated in the induction of interface dermatitis caused by Dsg3-specific T cells. This result is consistent with a previous study, in which H2K^b donor cells from *Il17a*$^{-/-}$ mice, when transferred into H2K$^{b/d}$ recipients, induced GVHD to an extent similar to *Il17a*$^{+/+}$ donor cells (42). However, it is still unclear whether IFN-γ directly acts against keratinocytes to cause tissue destruction or whether IFN-γ acts on T cells themselves to acquire cytotoxic activity. In a model of autoimmune diabetes utilizing NOD mice, IFN-γ was important to induce surface expression of FasL in β cells, which subsequently underwent apoptosis through Fas expressed by activated CD4$^+$ T cells (43). Furthermore, require-

ment of IFN-γ for induction of interface dermatitis implies that other Th1-associated molecules will be critically involved in this model. In addition to IFN-γ, IL-12 and IL-27 play pivotal roles in Th1 differentiation (44, 45). These cytokines participate in activation of molecules such as Jak1 and -2, and STAT1 and -4, all of which are important components of the signaling cascade that induces T-bet expression as well as IFN-γ expression or amplification. These critical molecules in Th1 differentiation may be potential targets to modulate disease activity, and our EAD model should provide a useful tool for in-depth evaluation.

Reported mouse models of TEN (46) and GVHD-like disease (47) target neoantigens in which transgenic mice that express membrane-bound ovalbumin, driven by the keratin 5 or 14 promoters, are transferred with OVA-specific $CD8^+$ T cells from OT-I mice. These mice demonstrated a role for $CD8^+$ T cells in inducing the TEN or GVHD-like phenotype and exhibited interface dermatitis on histology. Although $CD4^+$ T cells are likely involved in helping $CD8^+$ T cells, the roles of $CD4^+$ T cells in these models are unclear. Another report showed a local interface dermatitis model in which $CD5^+CD8^-$ allo-Ia-reactive T cell clones were injected subcutaneously and demonstrated that the immune response against the allo–MHC class II antigen was capable of inducing interface dermatitis (26). The Dsg3-specific TCRs we used are MHC class II–restricted, and these $CD4^+$ T cells were also capable of inducing interface dermatitis. Together, these results demonstrated that $CD4^+$ T cells are sufficient to induce interface dermatitis, at least in the acute phase, and suggest that MHC class II–expressing cells are important cell components in the pathological process.

A major issue in using neoantigen transgenic mice to analyze autoimmune responses is that the level of antigen expression cannot be controlled. Because these are nonfunctional molecules, it is possible that such molecules do not undergo physiological turnover or processing, including degradation and recycling. Studies of the immune reaction against neoantigens may not necessarily reflect the immune reaction against physiological antigens. We believe that the significance of the EAD that we report here lies in the fact that a physiological and functional molecule, which is expressed only in the skin and mucous membranes, is targeted. Dsg3 is also expressed in the thymus by Aire-expressing medullary thymic epithelial cells, and this may influence the output of immune reactions (48). Thus, the use of a physiological antigen as a target antigen of the autoimmune reaction may be important in analyzing autoimmunity. In this regard, Dsg3-specific TCR transgenic mice should provide a useful tool for exploring the development of autoreactive T cells in the thymus, as well as their maintenance or regulation in the periphery. How and where these cells interact with antigen-presenting cells and the processes by which they find their targets are fundamental, important questions in the context of not only PV and PNP, but also in the array of T cell–mediated inflammatory skin diseases that exhibit interface dermatitis.

In conclusion, we generated TCR transgenic mice with autoreactive $CD4^+$ T cells that are specific for Dsg3, a physiological autoantigen expressed by epidermal keratinocytes. The finding that $CD4^+$ T cells specific for a single skin-associated antigen could induce a PNP-like phenotype or interface dermatitis sheds light not only on the pathophysiology of pemphigus, but also on a range of other T cell–mediated inflammatory skin diseases with as-yet-undefined target antigens. This experimental model of autoimmune dermatitis should deepen our understanding of the immunopathophysiology of T cell–mediated skin diseases and provide impetus for investigating targeted autoantigens in human T cell–mediated skin diseases that exhibit interface dermatitis.

Methods

Mice. C57BL/6 (H-2^b, Ly-9.2) and 129/Sv mice (H-2^b, Ly-9.1) were purchased from CLEA Japan and Sankyo Labo Service Corporation. C57BL/6 *Rag2*$^{-/-}$ mice were purchased from the Central Institute for Experimental Animals (Tokyo, Japan). *Dsg3*$^{-/-}$ mice with a mixed 129/Sv and C57BL/6J genetic background and 129/Sv *Dsg3*$^{-/-}$ mice were obtained by mating male and female *Dsg3*$^{-/-}$ mice (Jackson Laboratory) (49). *Dsg1*$^{tg/tg}$*Dsg3*$^{-/-}$ mice with a C57BL/6 background were generated as described elsewhere (20). *Ifng*$^{-/-}$ mice were purchased from Jackson Laboratory. *Il17a*$^{-/-}$ mice were generated as described previously (42).

The animals were housed under specific pathogen–free conditions. The Keio University Ethics Committee for Animal Experiments approved all of the experiments in this study.

DNA construct for Dsg3-reactive TCR expression. Rearranged genes including the variable and junctional regions of the TCR-α and -β chains of a Dsg3-reactive T cell clone, 140#27 (Vα8-J21, Vβ6-Dβ1-Jβ1.3) (7), were obtained by RT-PCR using the following primers: Vα-Jα region, forward 5′-TCTCCCGGGTGCACTCAAGGACCAAGTGT-3′ (the *Xma*I site is underlined), reverse 5′-TTGGCTTCACTGTGAGCACGGTCCCA-3′; Vβ-Dβ-Jβ region, forward 5′-GTCTCGAGTTTCTCTTTTAACTAACTAATGCCC-3′ (*Xho*I), reverse 5′-CTACAACAATGAGCCGGCTTCCTT-3′. J21 or Jβ1.3 genes with an intron at their 3′ terminus were obtained from genomic DNA by PCR using the following primers: Jα21 intron, forward 5′-GGGGATGGGACCGTGCTCACAGTG-3′, reverse 5′-GCGCGGCCGCCCTGCCAGGAAGTCTAGTCAAAA-3′ (*Not*I); Jβ1.3 intron, forward 5′-GGAGAAGGAAGCCGGCTCATTGT-3′, reverse 5′-GCCCGCGGCGTAGGACTGTGAACAGTACAT-3′ (*Sac*II). The Vα-Jα and Vβ-Dβ-Jβ genes were linked with the Jα intron and Jβ intron to obtain Vα-Jα intron and Vβ-Dβ-Jβ intron genes, respectively, (Supplemental Figures 1 and 2) by linkage PCR. The genes of the TCR-α and -β chains of a Dsg3-reactive T cell clone, 162#24 (AV20S1-J39 and BV8S1-XDX-Jβ2.7), were obtained similarly by RT-PCR and linkage PCR using the following primers: Vα-Jα region, forward 5′-GCCCGGGGGAGAGATAACTCAAAGCTTCAGAGAAGA-3′ (*Xma*I), reverse 5′-GAGGTCTGACTCTCAAAATGGTTCCCAAGCCAAA-3′; Vβ-Dβ-Jβ region, forward 5′-GCTCGAGTAGTTCTGAGATGGGCTCCAGACTCTT-3′ (XhoI), reverse 5′-CTAAAACCGTGAGCCTGGTGCCGGGACCGAAGTA-3′. J39 or Jβ2.7 genes with an intron at their 3′ terminus were obtained from genomic DNA by PCR using the following primers: J39 intron, forward 5′-CTATGCAAACAAGATGATCTTTGGCTTGGGAA-3′, reverse 5′-GCCGCGGTCCAAGCTGTGGGCCACACCAGTGAATTT-3′ (*Sac*II); Jβ2.7 intron, forward 5′-ATGAACAGTACTTCGGTCCCGGCACCAGGCTCA-3′, reverse 5′-GCCGCGGCCCACCCAGTGCATGCATACCTCAGAGA-3′ (*Sac*II). Then, Vα-Jα and Vβ-Dβ-Jβ genes were linked with the Jα intron and Jβ intron to obtain Vα-Jα intron and Vβ-Dβ-Jβ intron genes, respectively. The genes of the TCR-α and -β chains of a Dsg3-reactive T cell clone, 164#2 (AV15S1-J45 and BV6S1-XDX-Jβ2.3), were obtained similarly by RT-PCR and linkage PCR using the following primers: Vα-Jα region, forward 5′-GCCCGGGCTTGCATGGCAAGAGATTGCAAGT-3′ (*Xma*I), reverse 5′-TTGGAGTCACAGTTAAGAGAGTTCCTTT-3′; Vβ-Dβ-Jβ region, forward 5′-GTCTCGAGTTTCTCTTTTAACTAACTAATGCCC-3′ (*Xho*I), reverse 5′-CGAGAACAGTCAGTCTGGTTCCT-3′. J45 or Jβ2.3 genes with an intron at their 3′ terminus were obtained from genomic DNA by PCR using the following primers: J45 intron, forward 5′-GGAGGCAGCAATTACAAACTGACAT-3′, reverse 5′-GCCGCGGCTGGATCCTGTATTCAATGTGCCTCCCT-3′ (*Sac*II); Jβ2.3 intron, forward 5′-GCAGAAACGCTGTATTTTGGCT-3′, reverse 5′-GCCGCGGCGAGGAGCCGAGTGCCTGGCCCAAA-3′ (*Sac*II).

Genes for the TCR-α and -β chains of 140#27, 162#24, and 164#2 were subcloned into expression cassettes for the TCR-α and -β chains, which were

provided by Diane Mathis (Harvard University, Cambridge, Massachusetts, USA) (50), following appropriate treatment with restriction enzymes. The nucleotide sequences of the restriction enzyme sites *Xho*I and *Kpn*I, which were originally contained in the TCR genes and used for subcloning and linearization before transfection, were altered using a QuikChange Multi Site-Directed Mutagenesis Kit (Stratagene), preserving the amino acid sequence.

Retroviral vector for Dsg3-reactive TCR expression. Complementary DNAs for the TCR-α and -β chains (Supplemental Figures 1–6) were isolated from the Dsg3-reactive T cell clones 140#27, 162#24, and 164#2 and inserted into the retroviral vector pMXs (51). The retroviral vector pMXs-IG harbors the sequence encoding GFP after the internal ribosomal entry sequence (IRES), and mock retroviral vector pMXs were used as negative controls.

Retroviral transduction. A packaging cell line, PLAT-E, was cultured in DMEM supplemented with 10% FCS, 2 mM L-glutamine, 1 mM pyruvate, 50 U/ml penicillin, 50 μg/ml streptomycin, 0.05 mM 2-ME, 1 μg/ml puromycin, and 10 μg/ml blasticidin. Retroviral vectors were transfected into packaging cell line PLAT-E cells and the supernatant was collected, as described previously (51). $CD4^+$ T cells were enriched from splenocytes of C57BL/6 mice by positive selection using the MACS cell separation system (Miltenyi Biotec) and then cultured in 24-well plates (10^6 cells/well) in complete medium (RPMI 1640 containing 10% FCS, 2 mM L-glutamine, 1 mM pyruvate, 50 U/ml penicillin, 50 μg/ml streptomycin, and 0.05 mM 2-ME) supplemented with 100 U/ml hIL-2 and 2.5 μg/ml Con A at 37°C for 24 hours. In some experiments, *Ifng*$^{-/-}$ and *Il17a*$^{-/-}$ mice were used as the source of $CD4^+$ T cells. The cells remaining after $CD4^+$ T cell enrichment were irradiated (30 Gy) and used for coculture with $CD4^+$ T cells as feeder cells. The activated $CD4^+$ T cells were resuspended in retroviral supernatant and centrifuged (1400 *g*, 1 hour, 30°C). After incubation at 37°C for 4 hours, the retroviral supernatant was removed, and the cells were cultured in complete medium supplemented with 100 U/ml hIL-2 at 37°C for 44 hours.

Generation of Dsg3-reactive TCR transgenic mice. Linearized transgenes of the TCR-α and -β chains for the T cell clone 140#27 were injected into fertilized oocytes of C57BL/6J (H-2^b) mice to generate TCR transgenic mice, C57BL/6J-Tg(Dsg3TCR140), which were maintained by mating with C57BL/6J mice. The line C57BL/6J-Tg(Dsg3TCR140)1 was referred to as Dsg3H1, and female Dsg3H1 mice were used in this study. Similarly, another TCR transgenic mouse, C57BL/6J-Tg(Dsg3TCR164)3, was generated by using transgenes of the TCR-α and -β chains for T cell clones, 164#2, and referred to as Dsg3L3 mice.

Peptide. We purchased 111 overlapping 15-mer peptides covering EC1 to EC3 of the Dsg3 extracellular domain (aa 1–394) from Sigma-Aldrich.

In vitro reconstitution of Dsg3-reactive TCR. The T cell hybridoma TG40-CD4 (52, 53) (provided by Takashi Saito, Riken Research Center for Allergy and Immunology, Yokohama, Japan) loses intrinsic TCR expression and expresses mouse CD4, which was retrovirally introduced. Then, 10 μg of linearized vectors for TCR-α and -β chain expression in addition to pSV2-hph (ATCC) containing the hygromycin-resistance gene were introduced into TG40-CD4 electrically (280 V, 0.975 μF). Stable transfectants were selected by using hygromycin after electroporation. The expression of transduced vectors was confirmed by flow cytometry, detecting coexpression of TCR-β and CD3, which is expressed as a complex with both the TCR-α and -β chains. Stable transfectants were sorted by a MACS cell isolation system using anti-TCRβ6 Ab-PE or anti-TCRβ8 Ab-PE (BD) in combination with anti-PE Ab microbeads (Miltenyi Biotech).

Reactivity of T cells and T cell hybridomas against Dsg3 peptides. A single-cell suspension of 4×10^4 cells was prepared from the spleens of TCR transgenic mice and cultured with 1×10^5 40 Gy–irradiated splenocytes and 10 μg/ml peptide in a 96-well round-bottom plate, and Dsg3-specific T cell proliferation was measured by ^{3}H-thymidine uptake, as described previously (54). 2×10^4 T cell hybridoma cells were cultured with 1×10^6 40 Gy–irradiated splenocytes and the peptide at the indicated concentration in 96-well flat-bottom plates for 24 hours. Subsequently, the culture supernatant was subjected to IL-2 ELISA (BD). Some of the experiments were performed in combination with anti-MHC class II mAb (M5/114) or isotype-matched rat mAb (BD).

Flow cytometry. A single-cell suspension of thymus, spleen, or lymph nodes from mice was stained appropriately using CD4-FITC, CD25-FITC, CD44-FITC, IL-17A–FITC, IFN-γ–FITC, TCR-β–PE, TCR-Vβ6–PE, CD4-PerCP-Cy5.5, CD8-PerCP-Cy5.5, 7-AAD, CD25-APC, CD24-APC, IL-4–APC, Foxp3-APC, CD45-APC/Cy7, CD4-PE/Cy7, CD62L-biotin, and CD229.1-biotin in combination with streptavidin-APC. The reagents in the anti-mouse/rat Foxp3 Staining Set (eBioscience) were used for intracellular staining following treatment with PMA, ionomycin, and brefeldin A (Sigma-Aldrich). For intracellular staining, 7-AAD was washed with PBS twice before fixation.

Generation of bone marrow chimeric mice. CD3-depleted BM cells from Dsg3H1 mice were prepared using CD3 microbeads (Miltenyi Biotech) and transferred intravenously into 7 Gy–irradiated 129/Sv mice or 129/Sv *Dsg3*$^{-/-}$ mice. Two months later, the recipient mice were used for further experiments.

Adoptive transfer. *Dsg3*$^{-/-}$ B cells were prepared from *Dsg3*$^{-/-}$ mice, as described previously (7). $CD4^+V\beta6^+$ T cells were prepared from the spleens and LNs of Dsg3H1 or Dsg3L3 mice by depleting $B220^+$ and $CD8^+$ cells, followed by positive selection of $V\beta6^+$ cells using the MACS cell separation system (Miltenyi Biotech). Then 5×10^6 *Dsg3*$^{-/-}$ B cells and 2.5×10^6 $CD4^+V\beta6^+$ T cells were transferred into *Rag2*$^{-/-}$ mice intravenously. In some experiments, retrovirally transduced $CD4^+$ T cells were transferred into *Rag2*$^{-/-}$ mice in combination with or without *Dsg3*$^{-/-}$ B cells. For CFSE labeling, $CD4^+$ T cells were isolated by depleting $B220^+$, $CD8^+$, Gr-1^+, and $CD11b^+$ cells from splenocytes and LN cells of Dsg3H1 mice by MACS and labeled with CFSE (Molecular Probes) before adoptive transfer, as described previously (7). Naive Ly9.1^-CD4^+ T cells derived from Dsg3H1→WT and Dsg3H1→*Dsg3*$^{-/-}$ mice, referred to as Dsg3H1→WT and Dsg3H1→*Dsg3*$^{-/-}$ $CD4^+$ T cells, respectively, were prepared by depleting Ly9.1^+, $B220^+$, $CD8^+$, Gr-1^+, $CD11b^+$, $DX5^+$, and $CD44^+$ cells from splenocytes and LN cells with magnetic beads, and $3–15 \times 10^5$ T cells were transferred with *Dsg3*$^{-/-}$ B cells into *Rag2*$^{-/-}$ mice.

Anti-Dsg3 Ab detection. Anti-Dsg3 IgG Ab was quantified by ELISA and detected by living cell staining, as described previously (49).

Immunoprecipitation-immunoblotting. Immunoprecipitation-immunoblotting was performed according to the previous report with some modification, in which we used primary mouse keratinocytes as a source of substrate (55).

Histological analysis. Formalin-fixed tissue was stained with H&E, and observed with an inverted TE2000-U microscope (Nikon). For immunofluorescent staining, 10-μm cryosections of the palate were fixed with acetone, and then stained with anti-mouse IgG Ab Alexa Fluor 488 (Molecular Probes), anti-TCRβ Ab-PE, and TOTO3 (Molecular Probes). Sections were observed under a confocal laser fluorescence FV1000 microscope (Olympus).

Statistics. Statistical analyses were made using the Mann-Whitney *U* test. Data represent mean ± SEM. $P < 0.05$ was considered significant.

Acknowledgments

We thank Diane Mathis (Harvard University) for the gift of cassette vectors for TCR-α and -β chain expression, Takashi Saito (Riken Research Center for Allergy and Immunology, Yokohama, Japan) for the TG40-CD4 T cell hybridoma cell line, Toshio Kitamura (Institute of Medical Science, University of Tokyo) for the pMXs retroviral vector and PLAT-E packaging cell line, H. Itoh for providing excellent animal care, and M. Suzuki for preparing the cryosections. This work was supported by Grants-in-Aid for Scientific Research from the Ministry of Education, Culture, Sports, Science and Technology of Japan; Health and Labor Sciences Research Grants for Research on Measures for Intractable Diseases from the Ministry of Health, Labor and Welfare of Japan;

the Uehara Memorial Foundation; and Keio Gijuku Academic Development Funds.
Received for publication February 1, 2011, and accepted in revised form June 11, 2011.

Address correspondence to: Masayuki Amagai, Department of Dermatology, Keio University School of Medicine, 35 Shinanomachi, Shinjuku-ku, Tokyo 160-8582, Japan. Phone: 81.3.5363.3822; Fax: 81.3.3351.6880; E-mail: amagai@a7.keio.jp.

1. Amagai M, Klaus-Kovtun V, Stanley JR. Autoantibodies against a novel epithelial cadherin in pemphigus vulgaris, a disease of cell adhesion. *Cell.* 1991;67(5):869–877.
2. Amagai M, Hashimoto T, Shimizu N, Nishikawa T. Absorption of pathogenic autoantibodies by the extracellular domain of pemphigus vulgaris antigen (Dsg3) produced by baculovirus. *J Clin Invest.* 1994;94(1):59–67.
3. Tsunoda K, et al. Induction of pemphigus phenotype by a mouse monoclonal antibody against the amino-terminal adhesive interface of desmoglein 3. *J Immunol.* 2003;170(4):2170–2178.
4. Amagai M. Autoimmune and infectious skin diseases that target desmogleins. *Proc Jpn Acad Ser B Phys Biol Sci.* 2010;86(5):524–537.
5. Raff MC. Role of thymus-derived lymphocytes in the secondary humoral immune response in mice. *Nature.* 1970;226(5252):1257–1258.
6. Garside P, Ingulli E, Merica RR, Johnson JG, Noelle RJ, Jenkins MK. Visualization of specific B and T lymphocyte interactions in the lymph node. *Science.* 1998;281(5373):96–99.
7. Takahashi H, Amagai M, Nishikawa T, Fujii Y, Kawakami Y, Kuwana M. Novel system evaluating in vivo pathogenicity of desmoglein 3-reactive T cell clones using murine pemphigus vulgaris. *J Immunol.* 2008;181(2):1526–1535.
8. Takahashi H, Kuwana M, Amagai M. A single helper T cell clone is sufficient to commit polyclonal naive B cells to produce pathogenic IgG in experimental pemphigus vulgaris. *J Immunol.* 2009; 182(3):1740–1745.
9. Anhalt GJ, et al. Paraneoplastic pemphigus. An autoimmune mucocutaneous disease associated with neoplasia. *N Engl J Med.* 1990;323(25):1729–1735.
10. Hoffman MA, Qiao X, Anhalt GJ. CD8+ T lymphocytes in bronchiolitis obliterans, paraneoplastic pemphigus, and solitary Castleman's disease. *N Engl J Med.* 2003;349(4):407–408.
11. Nikolskaia OV, Nousari CH, Anhalt GJ. Paraneoplastic pemphigus in association with Castleman's disease. *Br J Dermatol.* 2003;149(6):1143–1151.
12. Amagai M, Nishikawa T, Nousari HC, Anhalt GJ, Hashimoto T. Antibodies against desmoglein 3 (pemphigus vulgaris antigen) are present in sera from patients with paraneoplastic pemphigus and cause acantholysis in vivo in neonatal mice. *J Clin Invest.* 1998;102(4):775–782.
13. Anhalt GJ. Paraneoplastic pemphigus. *Adv Dermatol.* 1997;12:77–96.
14. Sontheimer RD. Lichenoid tissue reaction/interface dermatitis: clinical and histological perspectives. *J Invest Dermatol.* 2009;129(5):1088–1099.
15. Matsuoka LY. Graft versus host disease. *J Am Acad Dermatol.* 1981;5(5):595–599.
16. Pereira FA, Mudgil AV, Rosmarin DM. Toxic epidermal necrolysis. *J Am Acad Dermatol.* 2007; 56(2):181–200.
17. Oliver GF, Winkelmann RK, Muller SA. Lichenoid dermatitis: a clinicopathologic and immunopathologic review of sixty-two cases. *J Am Acad Dermatol.* 1989;21(2 pt 1):284–292.
18. Rudensky A, Preston-Hurlburt P, Hong SC, Barlow A, Janeway CA Jr. Sequence analysis of peptides bound to MHC class II molecules. *Nature.* 1991;353(6345):622–627.
19. Chicz RM, Urban RG, Gorga JC, Vignali DA, Lane WS, Strominger JL. Specificity and promiscuity among naturally processed peptides bound to HLA-DR alleles. *J Exp Med.* 1993;178(1):27–47.
20. Hata T, et al. Transgenic rescue of desmoglein 3 null mice with desmoglein 1 to develop a syngeneic mouse model for pemphigus vulgaris. *J Dermatol Sci.* 2011;63(1):33–39.
21. Weedon D. *Weedon's Skin Pathology.* Amsterdam, The Netherlands: Churchill Livingstone; 2009.
22. Bolognia JL, Jorizzo JL, Rapini RP. *Dermatology.* 2nd ed. Amsterdam, The Netherlands: Elsevier, Mosby, Saunders; 2008.
23. Akasu R, From L, Kahn HJ. Lymphocyte and macrophage subsets in active and inactive lesions of lichen planus. *Am J Dermatopathol.* 1993;15(3):217–223.
24. Freedberg IM, et al. *Fitzpatrick's Dermatology in General Medicine.* New York, New York, USA: McGraw-Hill Publishing; 1999.
25. Burns T, Breathnach S, Cox N, Griffiths C. *Rook's Textbook of Dermatology.* Oxford, United Kingdom: Wiley-Blackwell; 2005.
26. Shiohara T, Moriya N, Tsuchiya K, Nagashima M, Narimatsu H. Lichenoid tissue reaction induced by local transfer of Ia-reactive T-cell clones. *J Invest Dermatol.* 1986;87(1):33–38.
27. Lafaille JJ, Nagashima K, Katsuki M, Tonegawa S. High incidence of spontaneous autoimmune encephalomyelitis in immunodeficient anti-myelin basic protein T cell receptor transgenic mice. *Cell.* 1994;78(3):399–408.
28. Oyama N, et al. Autoantibodies to extracellular matrix protein 1 in lichen sclerosus. *Lancet.* 2003; 362(9378):118–123.
29. Baldo M, Bailey A, Bhogal B, Groves RW, Ogg G, Wojnarowska F. T cells reactive with the NC16A domain of BP180 are present in vulval lichen sclerosus and lichen planus. *J Eur Acad Dermatol Venereol.* 2010;24(2):186–190.
30. Sugerman PB, Satterwhite K, Bigby M. Autocytotoxic T-cell clones in lichen planus. *Br J Dermatol.* 2000;142(3):449–456.
31. McInnes IB, Schett G. Cytokines in the pathogenesis of rheumatoid arthritis. *Nat Rev Immunol.* 2007;7(6):429–442.
32. Bettelli E, Oukka M, Kuchroo VK. T(H)-17 cells in the circle of immunity and autoimmunity. *Nat Immunol.* 2007;8(4):345–350.
33. Lubberts E, et al. Treatment with a neutralizing anti-murine interleukin-17 antibody after the onset of collagen-induced arthritis reduces joint inflammation, cartilage destruction, and bone erosion. *Arthritis Rheum.* 2004;50(2):650–659.
34. Nakae S, Nambu A, Sudo K, Iwakura Y. Suppression of immune induction of collagen-induced arthritis in IL-17-deficient mice. *J Immunol.* 2003; 171(11):6173–6177.
35. Murphy CA, et al. Divergent pro- and antiinflammatory roles for IL-23 and IL-12 in joint autoimmune inflammation. *J Exp Med.* 2003;198(12):1951–1957.
36. Bending D, et al. Highly purified Th17 cells from BDC2.5NOD mice convert into Th1-like cells in NOD/SCID recipient mice. *J Clin Invest.* 2009; 119(3):565–572.
37. Wang B, et al. Interferon-gamma impacts at multiple points during the progression of autoimmune diabetes. *Proc Natl Acad Sci U S A.* 1997; 94(25):13844–13849.
38. Campbell IL, Kay TW, Oxbrow L, Harrison LC. Essential role for interferon-gamma and interleukin-6 in autoimmune insulin-dependent diabetes in NOD/Wehi mice. *J Clin Invest.* 1991;87(2):739–742.
39. Langrish CL, et al. IL-23 drives a pathogenic T cell population that induces autoimmune inflammation. *J Exp Med.* 2005;201(2):233–240.
40. O'Connor RA, et al. Cutting edge: Th1 cells facilitate the entry of Th17 cells to the central nervous system during experimental autoimmune encephalomyelitis. *J Immunol.* 2008;181(6):3750–3754.
41. Jager A, Dardalhon V, Sobel RA, Bettelli E, Kuchroo VK. Th1, Th17, and Th9 effector cells induce experimental autoimmune encephalomyelitis with different pathological phenotypes. *J Immunol.* 2009;183(11):7169–7177.
42. Nakae S, et al. Antigen-specific T cell sensitization is impaired in IL-17-deficient mice, causing suppression of allergic cellular and humoral responses. *Immunity.* 2002;17(3):375–387.
43. Amrani A, Verdaguer J, Thiessen S, Bou S, Santamaria P. IL-1alpha, IL-1beta, and IFN-gamma mark beta cells for Fas-dependent destruction by diabetogenic CD4(+) T lymphocytes. *J Clin Invest.* 2000;105(4):459–468.
44. Wilson CB, Rowell E, Sekimata M. Epigenetic control of T-helper-cell differentiation. *Nat Rev Immunol.* 2009;9(2):91–105.
45. Trinchieri G, Pflanz S, Kastelein RA. The IL-12 family of heterodimeric cytokines: new players in the regulation of T cell responses. *Immunity.* 2003;19(5):641–644.
46. Azukizawa H, et al. Induction of T-cell-mediated skin disease specific for antigen transgenically expressed in keratinocytes. *Eur J Immunol.* 2003; 33(7):1879–1888.
47. Shibaki A, Sato A, Vogel JC, Miyagawa F, Katz SI. Induction of GVHD-like skin disease by passively transferred CD8(+) T-cell receptor transgenic T cells into keratin 14-ovalbumin transgenic mice. *J Invest Dermatol.* 2004;123(1):109–115.
48. Wada N, et al. Aire-dependent thymic expression of desmoglein 3, the autoantigen in pemphigus vulgaris, and its role in T-cell tolerance. *J Invest Dermatol.* 2011;131(2):410–417.
49. Amagai M, Tsunoda K, Suzuki H, Nishifuji K, Koyasu S, Nishikawa T. Use of autoantigen-knockout mice in developing an active autoimmune disease model for pemphigus. *J Clin Invest.* 2000;105(5):625–631.
50. Kouskoff V, Signorelli K, Benoist C, Mathis D. Cassette vectors directing expression of T cell receptor genes in transgenic mice. *J Immunol Methods.* 1995;180(2):273–280.
51. Kitamura T, et al. Retrovirus-mediated gene transfer and expression cloning: powerful tools in functional genomics. *Exp Hematol.* 2003;31(11):1007–1014.
52. Sussman JJ, Saito T, Shevach EM, Germain RN, Ashwell JD. Thy-1- and Ly-6-mediated lymphokine production and growth inhibition of a T cell hybridoma require co-expression of the T cell antigen receptor complex. *J Immunol.* 1988; 140(8):2520–2526.
53. Zumla A, et al. Co-expression of human T cell receptor chains with mouse CD3 on the cell surface of a mouse T cell hybridoma. *J Immunol Methods.* 1992;149(1):69–76.
54. Kuwana M, Medsger TA Jr, Wright TM. T cell proliferative response induced by DNA topoisomerase I in patients with systemic sclerosis and healthy donors. *J Clin Invest.* 1995;96(1):586–596.
55. Hashimoto T, et al. Novel non-radioisotope immunoprecipitation studies indicate involvement of pemphigus vulgaris antigen in paraneoplastic pemphigus. *J Dermatol Sci.* 1998;17(2):132–139.

Effect of Bosentan on Systemic Sclerosis-associated Interstitial Lung Disease Ineligible for Cyclophosphamide Therapy: A Prospective Open-label Study

YOSHIAKI FURUYA and MASATAKA KUWANA

ABSTRACT. ***Objective.*** To evaluate the clinical benefits of the endothelin receptor antagonist bosentan on interstitial lung disease (ILD) in patients with systemic sclerosis (SSc) who are ineligible for cyclophosphamide (CYC) therapy.

Methods. In this prospective open-label study, 9 patients with SSc and ILD received bosentan for 24 months. The main reasons for avoiding CYC included severely impaired lung function, long disease duration, and relapse after CYC treatment. Pulmonary function tests and Doppler echocardiograms were evaluated every 6 months, and high-resolution computed tomography (HRCT) was performed every 12 months. For an extended survival analysis, 17 historical controls who met the inclusion criteria at referral and had not used any immunosuppressive or antifibrotic agents thereafter were selected from the SSc database.

Results. Two patients did not finish the study; one developed vasculitis requiring high-dose corticosteroids and another died of bacterial pneumonia. The remaining 7 patients tolerated bosentan and completed the study period. There were trends toward mildly reduced forced vital capacity, total lung capacity, and diffusing capacity for carbon monoxide over time. Two patients developed pulmonary hypertension during the 24-month period. HRCT scores for ground-glass opacity, pulmonary fibrosis, and honeycomb cysts gradually increased. In the extended study, there was no difference in cumulative survival rate between the bosentan-treated and historical control groups.

Conclusion. The gradual worsening of pulmonary function and HRCT findings in patients treated with bosentan was consistent with the natural course of SSc-associated ILD. This study does not support the use of bosentan for SSc-associated ILD even when CYC treatment is inadvisable. (First Release Sept 1 2011; J Rheumatol 2011;38:2186–92; doi:10.3899/jrheum.110499)

Key Indexing Terms:
SYSTEMIC SCLEROSIS
INTERSTITIAL LUNG DISEASE
PULMONARY HYPERTENSION
ENDOTHELINS

Interstitial lung disease (ILD) is the leading cause of disease-related morbidity and mortality in patients with systemic sclerosis (SSc)[1]. University of Pittsburgh database records of SSc-related deaths over the past 30 years show that the proportion of patients who died of ILD increased from 6% to 33%, indicating that ILD is the primary cause of SSc-related deaths today[2]. The current treatment for SSc-associated ILD (SSc-ILD) is limited to immunosuppressive agents. For patients with endstage ILD, lung transplantation may offer a viable alternative therapeutic option. A recent randomized placebo-controlled trial (Scleroderma Lung Study; SLS) reported a modest but significant benefit of oral cyclophosphamide (CYC) on lung function and health-related quality of life in SSc patients with active ILD[3], but this small effect was lost at 1 year of followup[4]. Two independent metaanalyses failed to demonstrate any clinically significant improvement in pulmonary function in patients with SSc who were treated with CYC[5,6]. In the Markov decision analytic model for evaluating risk-benefit tradeoffs, 1 year of CYC therapy for SSc-ILD actually resulted in a small loss in the quality-adjusted life-years compared with no CYC[7]. On the other hand, it has been reported that a clinical response to CYC is observed only in a subset of patients with ILD, with the predictors of clinical benefit including a forced vital capacity (FVC) < 70% and moderate pulmonary fibrosis on high-resolution computed tomography (HRCT)[8]. Therefore, the use of CYC should be decided on a patient-by-patient basis by considering the balance between therapeutic efficacy and potential toxicities, such as carcinogenesis and impaired fertility. Alternative reg-

From the Division of Rheumatology, Department of Internal Medicine, Keio University School of Medicine, Tokyo, Japan.

Dr. Kuwana receives a research grant for intractable diseases from the Japanese Ministry of Health, Labor and Welfare.

Y. Furuya, MD, PhD; M. Kuwana, MD, PhD, Division of Rheumatology, Department of Internal Medicine, Keio University School of Medicine.

Address correspondence to Dr. M. Kuwana, Division of Rheumatology, Department of Internal Medicine, Keio University School of Medicine, 35 Shinanomachi, Shinjuku-ku, Tokyo 160-8582, Japan.
E-mail: kuwanam@z5.keio.jp

Accepted for publication June 10, 2011.

imens for treating SSc-ILD are clearly needed, especially in patients with advanced or endstage ILD, significant risk for toxicity, or relapse after CYC treatment.

Endothelin-1 (ET-1), an endogenous vasoconstrictor, is implicated in the pathophysiology of pulmonary arterial hypertension (PAH) through the constriction and proliferation of vascular smooth muscle cells[9]. Endothelin receptor antagonists (ERA) such as bosentan have been shown to be effective treatments for PAH[10,11]. ET-1 also exerts profibrotic activity by modulating matrix turnover[12] and interacting with transforming growth factor-ß signaling[13]. In addition, ET-1 has been shown to play an important role in ILD pathogenesis, based on the elevated ET-1 levels in the plasma and bronchoalveolar lavage fluids of patients with ILD[14], and reduced collagen deposition in the lung with ERA treatment in a rat model for bleomycin-induced pulmonary fibrosis[15]. Due to its antifibrotic effects, ET-1 blockade would seem to be a logical approach to treating ILD, and randomized, placebo-controlled trials were conducted to investigate the potential efficacy of the dual ERA bosentan on idiopathic pulmonary fibrosis (BUILD-1)[16] and SSc-ILD (BUILD-2)[17]. Disappointingly, both trials failed to show improvement in the 6-min walk distance and in lung function in patients treated with bosentan, although there was a trend in favor of bosentan delaying the time to death or disease progression in patients with biopsy-proven usual interstitial pneumonia[16]. Since the BUILD-2 trial used strict criteria to select SSc patients with active and progressive ILD but without clinically apparent pulmonary hypertension (PH)[17], it is still possible that bosentan is effective for certain subsets of SSc-ILD, such as endstage ILD with severely impaired pulmonary function and complicating PH.

We conducted a 24-month open-label study to evaluate the clinical benefits of bosentan in patients with SSc-ILD ineligible for CYC treatment. The majority of patients enrolled did not satisfy the inclusion criteria of the BUILD-2 trial.

MATERIALS AND METHODS

Study design. This open-label prospective study was conducted at Keio University Hospital, Tokyo, Japan. The protocol was initiated in February 2006, and all the enrolled patients completed the study by February 2010. After assessing a patient's suitability for the study, bosentan was initiated at 62.5 mg twice daily. The dosage was increased to 125 mg twice daily at 4 weeks, and continued for 24 months. Patients were allowed other medications, with the exception of corticosteroids at a dose > 10 mg/day of prednisone or equivalent, or immunosuppressive agents. After completing the 24-month study period, patients were allowed to continue bosentan and were followed to assess the longterm survival and safety profiles. A complete medical history, physical examination, and laboratory analysis were performed for each patient at pretreatment, with more limited evaluations during monthly followup visits. Pulmonary function tests (PFT) and transthoracic echocardiography were done at the 0 (pretreatment), 6, 12, 18, and 24-month visits, and HRCT was performed at 0, 12, and 24 months. Safety profiles, including liver toxicity, were monitored at monthly intervals. The study protocol conformed to the ethical guidelines of the Declaration of Helsinki, as reflected in prior approval from the institutional review boards, and each patient gave informed written consent.

Subjects. Patients were considered for inclusion if they satisfied all the following criteria: they (1) were over 18 years of age; (2) met the American College of Rheumatology preliminary classification criteria for SSc[18]; (3) had both exertional dyspnea and ILD as determined by chest radiographs; and (4) were considered ineligible for CYC treatment because of severely impaired lung function [defined as having FVC < 45%, diffusing capacity for carbon monoxide (DLCO) < 30%, oxygen saturation measured by pulse oximetry < 85% during exercise], SSc duration > 7 years after the first non-Raynaud's phenomenon, a relapse after CYC treatment, a recent malignancy, or the patient's refusal[3]. Patients currently treated with corticosteroids > 10 mg/day prednisone or equivalent and/or immunosuppressive agents were excluded. For the extended survival analysis, we selected 17 historical controls from our SSc database, which contains information on 415 patients diagnosed since 1985, based on the following criteria: they (1) met the inclusion and exclusion criteria of this study at time of referral (first visit) to our hospital; and (2) had never been treated with immunosuppressive agents, corticosteroids > 10 mg/day (prednisone), or D-penicillamine since referral to our hospital. Patients with SSc were classified as having diffuse or limited cutaneous disease[19]. Diffuse cutaneous SSc (dcSSc) was considered present if, at any time during the course, skin thickening proximal to the elbows or knees was present, e.g., upper arms, thighs, anterior chest, or abdomen.

Outcome measures. PFT were performed to evaluate FVC, total lung capacity (TLC), and DLCO. Clinically significant worsening and improvement of PFT scores were defined as described[17]. Echocardiography using the Doppler technique was used to evaluate the degree of PH. The tricuspid regurgitation pressure gradient (TRPG) estimated by the tricuspid regurgitation peak velocity was recorded, with tricuspid regurgitation peak velocity > 3.4 m/s or TRPG > 46 mm Hg indicating the presence of PH[20]. The degree of ILD was semiquantitatively assessed by the HRCT scoring system proposed by Goldin, *et al*[21]. Scores (scale 0–24) for ground-glass opacity, pulmonary fibrosis, and honeycomb cysts were recorded individually. The ILD stage, extensive or limited disease, was determined according to the combined evaluation of PFT and HRCT[22]. The modified Rodnan skin thickness score (MRSS; scale 0–51), oral aperture, fingertip-to-palm distance (FTP), Raynaud's condition score (scale 0–10)[23], number of digital ulcers, and the Scleroderma Health Assessment Questionnaire (SHAQ) including the disability index (DI; scale 0–3) and visual analog scale (VAS; scale 0–3)[24,25] were also used to evaluate skin thickening, peripheral vascular disease, and functional status.

Identification of SSc-related antinuclear antibodies (ANA). Serum samples obtained from patients entering the study were analyzed for SSc-related ANA using indirect immunofluorescence and immunoprecipitation assays[26].

Statistical analysis. All continuous values were shown as the mean ± SD, and were compared using the Mann-Whitney U test. The frequencies between 2 groups were tested for statistical significance using the chi-square test or Fisher's 2-tailed exact test, when applicable. Changes in values at different timepoints from the baseline were compared by repeated measures analysis of variance. Cumulative survival rates were calculated according to the Kaplan-Meier method, and comparisons were made using the Cox-Mantel log-rank test.

RESULTS

Patient characteristics at baseline. Nine patients, with the baseline characteristics shown in Table 1, were enrolled. The ratio of men to women was 4:5, and age at entry ranged from 29 to 79 years (55 ± 19). Five were classified as having dcSSc. Evaluation of ANA profiles revealed that all patients with dcSSc were positive for antitopoisomerase I antibodies, and patients with limited cutaneous SSc had either anti-Th/To or anti-U1RNP antibodies. Based on the ILD staging system proposed by Goh, *et al*[22], all except 1 patient had extensive disease, and 4 patients were already receiving supplemental oxygen. Disease duration from the first non-Raynaud's symptom

Table 1. Baseline characteristics of the 9 patients with SSc enrolled.

Patient	Sex/Age at Entry, yrs	SSc Subset	ANA	ILD Stage*	Disease Duration†, mo	Data at Pretreatment % FVC	% TLC	% DLCO	TRPG, mmHg	MRSS	Reason for Not Using CYC
1	M 29	dcSSc	Topo I	E	25	53	62	44	36	30	Severely impaired lung function
2	F 63	dcSSc	Topo I	E	36	58	57	23	39	20	Relapse after CYC treatment
3	F 65	dcSSc	Topo I	E	293	65	76	30	25	7	Long disease duration
4	M 36	dcSSc	Topo I	E	36	44	53	53	29	14	Severely impaired lung function
5	F 54	dcSSc	Topo I	E	297	34	42	18	53	25	Severely impaired lung function
6	M 62	lcSSc	Th/To	E	167	24	37	16	38	2	Severely impaired lung function
7	F 31	lcSSc	U1RNP	E	72	62	68	22	30	2	Patient refusal
8	M 77	lcSSc	U1RNP	L	10	77	67	40	27	4	Recent malignancy
9	F 79	lcSSc	U1RNP	E	338	107	81	34	30	2	Long disease duration

* E: extensive disease; L: limited disease. † Disease duration from first non-Raynaud's phenomenon. SSc: systemic sclerosis; dcSSc: diffuse cutaneous SSc: lcSSc: limited cutaneous SSc; ANA: antinuclear antibody; TOPO I: topoisomerase I; U1RNP: U1 ribonucleoprotein; FVC: forced vital capacity; TLC: total lung capacity; DLCO: diffusing capacity for carbon monoxide; TRPG: tricuspid regurgitation pressure gradient; MRSS: modified Rodnan skin thickness score; CYC: cyclophosphamide.

ranged from 10 to 338 months (141 ± 134). Patient 5 showed elevated TRPG (53 mmHg), suggesting the coexistence of PH. CYC was not used due to severely impaired lung function in 4 patients, long disease duration in 2, relapse after CYC treatment in 1, the patient's refusal in 1, and recent malignancy in 1.

Safety profiles. During the 24-month study, none of the patients experienced elevated aminotransferase levels (> 3-fold the upper limit of normal) or other adverse events potentially associated with bosentan. Two patients were dropped from the study; 1 because of antineutrophil cytoplasmic antibody-associated vasculitis requiring high-dose corticosteroid therapy at 7 months (Patient 3) and another died of bacterial pneumonia at 17 months (Patient 6). The remaining 7 patients tolerated bosentan and completed the entire study period.

Serial evaluations of outcome measures. Serial measurements of FVC, TLC, DLCO, and TRPG in the 9 patients enrolled are shown in Figure 1. In the 7 patients who completed the 24-month study period, there were trends toward mildly reduced FVC (62.1% ± 24.0% at baseline to 58.7% ± 22.8% at 24 months), %TLC (61.4% ± 12.4% at baseline to 56.0% ± 10.9% at 24 months), and %DLCO (33.4% ± 13.0% at baseline to 27.6% ± 16.4% at 24 months), but only the reduction of TLC was statistically significant ($p = 0.04$). The PFT scores remained stable for all but 1 patient (Patient 9), who experienced clinically significant worsening at 12 and 24 months. None of the patients showed improved PFT scores. TRPG changes were not statistically significant (34.9 ± 9.0 at baseline to 35.4 ± 18.2 at 24 months), but in 2 patients who experienced increased TRPG (Patients 2 and 5), PH was confirmed by right-heart catheterization.

Serial HRCT evaluations revealed stable but slightly increased scores for ground-glass opacity and pulmonary fibrosis (Table 2). The scores for honeycomb cysts gradually increased, and had doubled at 24 months compared with the pretreatment scores ($p = 0.02$). As shown in Table 2, the MRSS and oral aperture were stable, but flexion contractures of the digits as measured by FTP appeared to worsen during the study period. The Raynaud's condition scores tended to increase, but 3 patients experienced a decrease in the number of digital ulcers at 12 and 24 months compared to those observed at pretreatment. There was no treatment effect for the SHAQ-DI or VAS during the study period.

Extended survival analysis. Seven patients continued to take bosentan for an additional 2–24 months after the 24-month study period. None of the patients stopped bosentan due to a potential adverse event during the extension period. Sildenafil was added in 2 patients with PH; one of these died of respiratory failure at 27 months. Therefore, 2 patients (22%) died of ILD-related causes (respiratory tract infection at 17 months and respiratory failure at 27 months) while taking bosentan. The cumulative survival rate in patients treated with bosentan at 2 and 3 years was 86% and 71%, respectively (Figure 2).

We further compared the cumulative survival rate in bosentan-treated patients and historical controls. Table 3 shows baseline characteristics in the 9 bosentan-treated patients and 17 historical controls. There was no statistically significant difference in age at entry, disease duration, or lung function such as FVC and DLCO, but historical controls appeared to be more homogeneous than bosentan-treated patients: historical controls had shorter disease duration, lower %FVC, and higher prevalence of antitopoisomerase I antibody. When an out-